Accepted Manuscript

Title: Free Vibrations of Four-Parameter Functionally Graded Parabolic Panels and Shells of Revolution

Authors: Francesco Tornabene, Erasmo Viola

PII: S0997-7538(09)00054-0

DOI: 10.1016/j.euromechsol.2009.04.005

Reference: EJMSOL 2522

To appear in: *European Journal of Mechanics / A Solids*

Received Date: 19 May 2008

Revised Date: 4 February 2009

Accepted Date: 16 April 2009

Please cite this article as: Tornabene, F., Viola, E. Free Vibrations of Four-Parameter Functionally Graded Parabolic Panels and Shells of Revolution, European Journal of Mechanics / A Solids (2009), doi: 10.1016/j.euromechsol.2009.04.005

This is a PDF file of an unedited manuscript that has been accepted for publication. As a service to our customers we are providing this early version of the manuscript. The manuscript will undergo copyediting, typesetting, and review of the resulting proof before it is published in its final form. Please note that during the production process errors may be discovered which could affect the content, and all legal disclaimers that apply to the journal pertain.

FREE VIBRATIONS OF FOUR-PARAMETER FUNCTIONALLY GRADED PARABOLIC PANELS AND SHELLS OF REVOLUTION

Francesco Tornabene[1*], Erasmo Viola[1]

[1] DISTART - Department, Faculty of Engineering, University of Bologna

Keywords: Functionally Graded Materials, Doubly Curved Shells, FSD Theory, Free Vibrations, Generalized Differential Quadrature.

Abstract. Basing on the First-order Shear Deformation Theory (FSDT), this paper focuses on the dynamic behaviour of moderately thick functionally graded parabolic panels and shells of revolution. A generalization of the power-law distribution presented in literature is proposed. Two different four parameter power-law distributions are considered for the ceramic volume fraction. Some symmetric and asymmetric material profiles through the functionally graded shell thickness are illustrated by varying the four parameters of power-law distributions. The governing equations of motion are expressed as functions of five kinematic parameters. For the discretization of the system equations the Generalized Differential Quadrature (GDQ) method has been used. Numerical results concerning four types of parabolic shell structures illustrate the influence of the parameters of the power-law distribution on the mechanical behaviour of shell structures considered.

ACCEPTED MANUSCRIPT

* Corresponding author, Tel.: +39-051-209-3379; Fax: +39-051-209-3495
E-mail address: francesco.tornabene@mail.ing.unibo.it

1. Introduction

Functionally graded materials (FGM) are a class of composites that have a smooth and continuous variation of material properties from one surface to another and thus can alleviate the stress concentrations found in laminated composites. Typically, these materials consist of a mixture of ceramic and metal, or a combination of different materials. Extensive research work has been carried out on this new class of composites since the concept itself was first introduced and proposed in the late 1980s in Japan. One of the advantages of using functionally graded materials is that they can survive environments with high temperature gradients, while maintaining structural integrity. Furthermore, the continuous change in the compositions leads to a smooth change in the mechanical properties, which has many advantages over the laminated composites, where the delamination and cracks are most likely to initiate at the interfaces due to the abrupt variation in mechanical properties between laminae.

In the last years, some researchers have analyzed various characteristics of functionally graded structures (Ng et al., 2000; Yang et al., 2003; Della Croce and Venini, 2004; Liew et al., 2004; Wu and Tsai, 2004; Elishakoff et al., 2005; Patel et al., 2005; Abrate, 2006; Pelletier and Vel, 2006; Zenkour, 2006; Arciniega and Reddy, 2007; Nie and Zhong, 2007; Roque et al., 2007; Yang and Shen, 2007).

The aim of this paper is to study the dynamic behaviour of functionally graded parabolic shell structures derived from shells of revolution, which are very common structural elements. As a matter of fact, the approach for studying the vibration of isotropic shell (Tornabene and Viola, 2008) is now extended to shells made of four parametric functionally graded materials.

The work is based on the First-order Shear Deformation Theory (FSDT) (Reddy, 2003). The geometric model refers to a moderately thick shell, and the effects of transverse shear deformation as well as rotary inertia are taken into account. Several studies have been presented earlier for the vibration analysis of such revolution shells and the most popular numerical tool in carrying out these analyses was the finite element method (Reddy, 2003). The generalized collocation method based on the ring element method has also been applied. With regard to the latter method, each static and kinematic variable is transformed into a theoretically infinite Fourier series of harmonic components, with respect to the circumferential co-ordinate (Viola and Artioli, 2004; Artioli et al., 2005; Artioli and Viola, 2005, 2006). In other words, when dealing with a completely closed shell, the 2-D problem can be reduced using standard Fourier decomposition. In a panel, however, it is not possible to perform such a reduction operation, and the two-dimensional field must be directly dealt with. In this paper, the governing equations of motion are a set of five two-dimensional partial differential equations with variable coefficients. These fundamental equations are expressed in terms of kinematic parameters and can be obtained by combining the three basic sets of equations, namely equilibrium, kinematic and constitutive equations.

ACCEPTED MANUSCRIPT

This paper is motivated by the lack of studies in the technical literature about the free vibration analysis of functionally graded parabolic panels and shells and the effect of the power-law distribution on their mechanical behaviour.

Firstly, two different power-law variations of the volume fraction of the constituents in the thickness direction are proposed. The effect of the power-law exponent and of the power-law distribution choice on the mechanical behaviour of functionally graded parabolic panels and shells is investigated.

Symmetric and asymmetric volume fraction profiles are presented in this paper. Classical volume fraction profiles can be obtained as special cases of the general distribution laws presented in this work. For the first power-law distribution, the bottom surface of the structure is ceramic rich, whereas the top surface can be metal rich, ceramic rich or made of a mixture of the two constituents and, on the contrary, for the second power-law distribution. The homogeneous isotropic material can be regarded as a special case of functionally graded materials, too. From this point of view, the present work generalizes the paper by Tornabene and Viola (2008).

Secondly, another aim of the present paper is to demonstrate an efficient application of the differential quadrature approach (Viola and Tornabene, 2005; Tornabene, 2007; Tornabene and Viola, 2007, 2008; Viola et al., 2007; Marzani et al. 2008), by solving the equations of motion governing the free vibration of functionally graded thick parabolic panels and shells of revolution.

The system of second-order linear partial differential equations is solved without resorting to the one-dimensional formulation of the dynamic equilibrium of the shell. The discretization of the system by means of the Generalized Differential Quadrature method (GDQ) leads to a standard linear eigenvalue problem, where two independent variables are involved. In this way, it is possible to compute the complete assessment of the modal shapes corresponding to natural frequencies of panel structures. It should be noted that there is comparatively little literature available for these structures, compared to literature on the free vibration analysis of complete shells of revolution. In this study, complete revolution shells are obtained as special cases of shell panels by satisfying the kinematic and physical compatibility at the common meridian with $\vartheta = 0, 2\pi$.

2. Fundamental System for Functionally Graded Panels and Shells of Revolution

The basic configuration of the problem considered here is a doubly curved shell as shown in Fig. 1. The co-ordinates along the meridian and circumferential directions of the reference surface are φ and s, respectively. The distance of each point from the shell mid-surface along the normal is ζ. The shells considered are assumed to be single-layer shells of uniform thickness h. It is worth noting that, differently from the work by Tornabene and Viola (2008), the

ACCEPTED MANUSCRIPT

co-ordinates of the shell reference surface are changed $\left((\varphi,\vartheta)\rightarrow(\varphi,s)\right)$ in order to simplify the fundamental equations. Now, all the geometric relations and fundamental equations are re-written following the new co-ordinate system.

The angle formed by the external normal **n** to the reference surface and the axis of rotation x_3, or the geometric axis x_3' of the meridian curve, is defined as the meridian angle φ and the angle between the radius of the parallel circle $R_0(\varphi)$ and the x_1 axis is designated as the circumferential angle ϑ as shown in Fig. 2. The parametric co-ordinates (φ,s) define the meridian curves and the parallel circles upon the middle surface of the shell, respectively. The curvilinear abscissa $s(\varphi)$ of a generic parallel is related to the circumferential angle ϑ by the relation $s=\vartheta R_0$. The position of an arbitrary point within the shell material is known by the co-ordinates φ $\left(\varphi_0\le\varphi\le\varphi_1\right)$, s $\left(0\le s\le s_0\right)$ upon the middle surface, and ζ directed along the outward normal **n** and measured from the reference surface $\left(-h/2\le\zeta\le h/2\right)$.

The geometry of shells considered is a surface of revolution with a parabolic curved meridian. The parabolic meridian can be described with the following equation:

$$\left(R_0-R_b\right)^2-kx_3'=0 \tag{1}$$

where $k=\left(s_1^2-d^2\right)/S$ is a characteristic parameter of the parabolic curve. The horizontal radius $R_0(\varphi)$ of a generic parallel of the shell represents the distance of each point from the axis of revolution and for a shell with parabolic meridian assumes the form $R_0(\varphi)=k\tan\varphi/2+R_b$. R_b is the shift of the geometric axis of the meridian x_3' with reference to the axis of revolution x_3.

The radii of curvature $R_\varphi(\varphi)$, $R_s(\varphi)$ in the meridian and circumferential directions and the first derivative of $R_\varphi(\varphi)$ with respect to φ can be expressed according to the well known differential geometry formulae.

As regards shell theory, this work is based on the following assumptions: (1) the transverse normal is inextensible so that the normal strain is equal to zero: $\varepsilon_n=\varepsilon_n(\varphi,s,\zeta,t)=0$; (2) the transverse shear deformation is supposed to influence the governing equations so that normal lines to the reference surface of the shell before deformation remain straight, but not necessarily normal after deformation (a relaxed Kirchhoff-Love hypothesis); (3) the shell deflections are small and the strains are infinitesimal; (4) the shell is moderately thick and therefore it is possible to assume that the thickness-direction normal stress is negligible so that the plane assumption can be invoked:

ACCEPTED MANUSCRIPT

$\sigma_n = \sigma_n(\varphi, s, \zeta, t) = 0$; (5) the linear elastic behaviour of anisotropic materials is assumed; (6) the rotary inertia is also taken into account.

Consistent with the assumptions of a moderately thick shell theory reported above, the displacement field considered in this study is that of the First-order Shear Deformation Theory and can be expressed in the following, well known, form:

$$\begin{aligned} U_\varphi(\varphi, s, \zeta, t) &= u_\varphi(\varphi, s, t) + \zeta\beta_\varphi(\varphi, s, t) \\ U_s(\varphi, s, \zeta, t) &= u_s(\varphi, s, t) + \zeta\beta_s(\varphi, s, t) \\ W(\varphi, s, \zeta, t) &= w(\varphi, s, t) \end{aligned} \tag{2}$$

where u_φ, u_s, w are the displacement components of points lying on the middle surface $(\zeta = 0)$ of the shell, along meridian, circumferential and normal directions, respectively, while t is the time variable. β_φ and β_s represent normal-to-mid-surface rotations. The kinematic hypothesis expressed by equations (2) should be supplemented by the statement that the shell deflections are small and strains are infinitesimal, that is $w(\varphi, s, t) \ll h$. It is worth noting that in-plane displacements U_φ and U_s vary linearly through the thickness, while W remains independent of ζ.

Relationships between strains and displacements along the shell reference (middle) surface $(\zeta = 0)$ and the five equations of dynamic equilibrium in terms of internal actions can be written as in Tornabene and Viola (2008).

As far as the constitutive relations for a functionally graded linear elastic material are concerned, they relate internal stress resultants and internal couples with generalized strain components on the middle surface:

$$\begin{bmatrix} N_\varphi \\ N_s \\ N_{\varphi s} \\ M_\varphi \\ M_s \\ M_{\varphi s} \\ T_\varphi \\ T_s \end{bmatrix} = \begin{bmatrix} A_{11} & A_{12} & 0 & B_{11} & B_{12} & 0 & 0 & 0 \\ A_{12} & A_{11} & 0 & B_{12} & B_{11} & 0 & 0 & 0 \\ 0 & 0 & A_{66} & 0 & 0 & B_{66} & 0 & 0 \\ B_{11} & B_{12} & 0 & D_{11} & D_{12} & 0 & 0 & 0 \\ B_{12} & B_{11} & 0 & D_{12} & D_{11} & 0 & 0 & 0 \\ 0 & 0 & B_{66} & 0 & 0 & D_{66} & 0 & 0 \\ 0 & 0 & 0 & 0 & 0 & 0 & \kappa A_{66} & 0 \\ 0 & 0 & 0 & 0 & 0 & 0 & 0 & \kappa A_{66} \end{bmatrix} \begin{bmatrix} \varepsilon_\varphi^0 \\ \varepsilon_s^0 \\ \gamma_{\varphi s}^0 \\ \chi_\varphi \\ \chi_s \\ \chi_{\varphi s} \\ \gamma_{\varphi n} \\ \gamma_{sn} \end{bmatrix} \tag{3}$$

where κ is the shear correction factor, which is usually taken as $\kappa = 5/6$, such as in the present work. In particular, it is worth noting that the determination of shear correction factors for composite laminated structures is still an unsolved issue, because these factors depend on various parameters (Alfano et al., 2001; Auricchio and Sacco, 1999, 2003).

In equations (3) the three components $N_\varphi, N_s, N_{\varphi s}$ are the in-plane meridian, circumferential and shearing force

ACCEPTED MANUSCRIPT

resultants, $M_\varphi, M_s, M_{\varphi s}$ are the analogous couples, while T_φ, T_s are the transverse shear force resultants. We notice that, in the above definitions (3) the symmetry of shearing force resultants $N_{\varphi s}, N_{s\varphi}$ and torsional couples $M_{\varphi s}, M_{s\varphi}$ is assumed as a further hypothesis, even if it is satisfied only in the case of spherical shells and flat plates (Toorani and Lakis, 2000). This assumption is derived from the consideration that ratios $\zeta/R_\varphi, \zeta/R_s$ can be neglected with respect to unity ($\zeta/R_\varphi, \zeta/R_s \ll 1$). Moreover, the first three strains $\varepsilon_\varphi^0, \varepsilon_s^0, \gamma_{\varphi s}^0$ are in-plane meridian, circumferential and shearing components and $\chi_\varphi, \chi_s, \chi_{\varphi s}$ are the corresponding analogous curvature changes. The last two components $\gamma_{\varphi n}, \gamma_{sn}$ are the transverse shearing strains.

The extensional stiffnesses A_{ij}, the bending stiffnesses D_{ij} and the bending-extensional coupling stiffnesses B_{ij} are defined as:

$$A_{ij} = \int_{-\frac{h}{2}}^{\frac{h}{2}} Q_{ij}(\zeta)\, d\zeta, \quad B_{ij} = \int_{-\frac{h}{2}}^{\frac{h}{2}} Q_{ij}(\zeta)\, \zeta\, d\zeta, \quad D_{ij} = \int_{-\frac{h}{2}}^{\frac{h}{2}} Q_{ij}(\zeta)\, \zeta^2 d\zeta \tag{4}$$

where the elastic constants $Q_{ij} = Q_{ij}(\zeta)$ are functions of thickness coordinate ζ and are represented by the following:

$$Q_{11} = \frac{E(\zeta)}{1-\left(\nu(\zeta)\right)^2}, \quad Q_{12} = \frac{\nu(\zeta)E(\zeta)}{1-\left(\nu(\zeta)\right)^2}, \quad Q_{66} = \frac{E(\zeta)}{2\left(1+\nu(\zeta)\right)} \tag{5}$$

Typically, the functionally graded materials are made of a mixture of two constituents. In this work, it is assumed that the functionally graded material is made of a mixture of a ceramic and metal constituent. The material properties of the functionally graded shell vary continuously and smoothly along the thickness direction ζ and are functions of the volume fractions and properties of the constituent materials. The Young's modulus $E(\zeta)$, Poisson's ratio $\nu(\zeta)$ and mass density $\rho(\zeta)$ of the functionally graded shell can be expressed as a linear combination:

$$\begin{aligned} \rho(\zeta) &= (\rho_C - \rho_M)V_C + \rho_M \\ E(\zeta) &= (E_C - E_M)V_C + E_M \\ \nu(\zeta) &= (\nu_C - \nu_M)V_C + \nu_M \end{aligned} \tag{6}$$

where ρ_C, E_C, ν_C, V_C and ρ_M, E_M, ν_M, V_M represent mass density, Young's modulus, Poisson's ratio and volume fraction of the ceramic and metal constituent materials, respectively.

In this paper, the ceramic volume fraction V_C follows two simple four parameter power-law distributions:

ACCEPTED MANUSCRIPT

$$
\begin{aligned}
FGM_{1\,(a/b/c/p)}:\ \ V_C &= \left(1-a\left(\frac{1}{2}+\frac{\zeta}{h}\right)+b\left(\frac{1}{2}+\frac{\zeta}{h}\right)^{c}\right)^{p} \\
FGM_{2\,(a/b/c/p)}:\ \ V_C &= \left(1-a\left(\frac{1}{2}-\frac{\zeta}{h}\right)+b\left(\frac{1}{2}-\frac{\zeta}{h}\right)^{c}\right)^{p}
\end{aligned}
\tag{7}
$$

where the volume fraction index p $(0 \le p \le \infty)$ and the parameters a,b,c dictate the material variation profile through the functionally graded shell thickness. It is worth noting that the volume fractions of all the constituent materials should add up to unity:

$$
V_C + V_M = 1 \tag{8}
$$

In order to choose the three parameters a,b,c in a suitable way, the relation (8) must be always satisfied for every volume fraction index p. By considering the relations (7), when the power-law exponent is set equal to zero ($p=0$) or equal to infinity ($p=\infty$), the homogeneous isotropic material is obtained (Tornabene and Viola, 2008) as a special case of the functionally graded material. In fact, from equations (8), (7) and (6) it is possible to obtain:

$$
\begin{aligned}
&p=0 \rightarrow V_C=1, V_M=0 \rightarrow \rho(\zeta)=\rho_C,\ E(\zeta)=E_C,\ \nu(\zeta)=\nu_C \\
&p=\infty \rightarrow V_C=0, V_M=1 \rightarrow \rho(\zeta)=\rho_M,\ E(\zeta)=E_M,\ \nu(\zeta)=\nu_M
\end{aligned}
\tag{9}
$$

Some material profiles through the functionally graded shell thickness are illustrated in Figs. 3, 4 and 5. In Fig. 3 the classical volume fraction profiles, such as reported in literature, are presented as special cases of the general distribution laws (7) by setting $a=1$ and $b=0$. As can be seen from Fig. 3(a), for the first distribution $FGM_{1\,(a=1/b=0/c/p)}$ (7) the material composition is continuously varied such that the bottom surface ($\zeta/h=-0.5$) of the shell is ceramic rich, whereas the top surface ($\zeta/h=0.5$) is metal rich. Fig. 3(b) shows that conversely, for the second distribution $FGM_{2\,(a=1/b=0/c/p)}$ (7) the top surface ($\zeta/h=0.5$) of the shell is ceramic rich, whereas the bottom surface ($\zeta/h=-0.5$) is metal rich. Choosing other values for the parameters a,b,c, it is possible to obtain symmetric and asymmetric volume fraction profiles as shown in Figs. 4 and 5. In Figs. 4(a) and 4(b), by setting $a=1$, $b=1$ and $c=2$ the two distributions $FGM_{1\,(a=1/b=1/c=2/p)}$, $FGM_{2\,(a=1/b=1/c=2/p)}$ (7) present the same profiles by varying the volume fraction index p and are symmetric respect to the reference surface ($\zeta/h=0$) of the shell. Furthermore, these distributions are characterized by the fact that both the top ($\zeta/h=0.5$) and bottom surface ($\zeta/h=-0.5$) are ceramic rich, while there is a mixture of two constituents through the thickness. Figs. 4(c) and 4(d) illustrate asymmetric profiles $FGM_{1\,(a=1/b=1/c=4/p)}$, $FGM_{2\,(a=1/b=1/c=4/p)}$ (7) obtained by setting $a=1$, $b=1$ and $c=4$. As

ACCEPTED MANUSCRIPT

shown by the figures being reviewed, we have the same constituent at the top and bottom surface but, unlike the previous cases (Figs. 4(a) and 4(b)), profiles are not symmetric with respect to the reference surface ($\zeta/h=0$) of the shell. Fig. 5 shows other cases obtained by varying the parameters a,b,c . These profiles are characterized by the fact that one of the two shell surfaces (the top or bottom surface) presents a mixture of two constituents. For example, by considering the $FGM_{1\,(a=1/b=0.5/c=4/p=1)}$ distribution (Fig. 5(a)), at the top surface we have a mixture of ceramic and metal made up by fifty per cent of ceramic and fifty per cent of metal, while the bottom surface ($\zeta/h=-0.5$) is ceramic rich. Figs. 5(b), (c), (d), (e) and (f) illustrate various power-law distribution cases obtained by modifying the parameters a,b,c,p . From a design point of view it is important to know if the top surface of the shell ($\zeta/h=0.5$) is ceramic or metal rich, if the bottom surface ($\zeta/h=-0.5$) is metal or ceramic rich, or if one of these surfaces presents a mixture of two constituents. One of the aim of this work is to propose a generalization of the power-law distribution presented in literature and to illustrate the influence of the power-law exponent p and of the choice of the parameters a,b,c on the mechanical behaviour of shell structures.

The three basic sets of equations, namely the kinematic, constitutive and equilibrium equations may be combined to give the fundamental system of equations, also known as the governing system of equations. By substituting the kinematic equations into the constitutive equations and the result of this substitution into the equilibrium equations, the complete equations of motion in terms of displacements can be written as:

$$\begin{bmatrix} L_{11} & L_{12} & L_{13} & L_{14} & L_{15} \\ L_{21} & L_{22} & L_{23} & L_{24} & L_{25} \\ L_{31} & L_{32} & L_{33} & L_{34} & L_{35} \\ L_{41} & L_{42} & L_{43} & L_{44} & L_{45} \\ L_{51} & L_{52} & L_{53} & L_{54} & L_{55} \end{bmatrix} \begin{bmatrix} u_\varphi \\ u_s \\ w \\ \beta_\varphi \\ \beta_s \end{bmatrix} = \begin{bmatrix} I_0 & 0 & 0 & I_1 & 0 \\ 0 & I_0 & 0 & 0 & I_1 \\ 0 & 0 & I_0 & 0 & 0 \\ I_1 & 0 & 0 & I_2 & 0 \\ 0 & I_1 & 0 & 0 & I_2 \end{bmatrix} \begin{bmatrix} \ddot{u}_\varphi \\ \ddot{u}_s \\ \ddot{w} \\ \ddot{\beta}_\varphi \\ \ddot{\beta}_s \end{bmatrix} \tag{10}$$

where the explicit forms of the equilibrium operators $L_{ij},\ i,j=1,...,5$ are listed in Appendix and the mass inertias assumed the following form:

$$I_i = \int_{-\frac{h}{2}}^{\frac{h}{2}} \rho(\zeta)\zeta^i \left(1+\frac{\zeta}{R_\varphi}\right)\left(1+\frac{\zeta}{R_s}\right) d\zeta, \quad i=0,1,2 \tag{11}$$

Three kinds of boundary conditions are considered, namely the fully clamped edge boundary condition (C), the simply supported edge boundary condition (S) and the free edge boundary condition (F). The equations describing the boundary conditions can be written as follows:

ACCEPTED MANUSCRIPT

Clamped edge boundary condition (C)

$$u_\varphi = u_s = w = \beta_\varphi = \beta_s = 0 \quad \text{at } \varphi = \varphi_0 \text{ or } \varphi = \varphi_1, \quad 0 \le s \le s_0 \tag{12}$$

$$u_\varphi = u_s = w = \beta_\varphi = \beta_s = 0 \quad \text{at } s = 0 \text{ or } s = s_0, \quad \varphi_0 \le \varphi \le \varphi_1 \tag{13}$$

Simply supported edge boundary condition (S)

$$u_\varphi = u_s = w = \beta_s = 0, \quad M_\varphi = 0 \quad \text{at } \varphi = \varphi_0 \text{ or } \varphi = \varphi_1, \quad 0 \le s \le s_0 \tag{14}$$

$$u_\varphi = u_s = w = \beta_\varphi = 0, \quad M_s = 0 \quad \text{at } s = 0 \text{ or } s = s_0, \quad \varphi_0 \le \varphi \le \varphi_1 \tag{15}$$

Free edge boundary condition (F)

$$N_\varphi = N_{\varphi s} = T_\varphi = M_\varphi = M_{\varphi s} = 0 \quad \text{at } \varphi = \varphi_0 \text{ or } \varphi = \varphi_1, \quad 0 \le s \le s_0 \tag{16}$$

$$N_s = N_{\varphi s} = T_s = M_s = M_{\varphi s} = 0 \quad \text{at } s = 0 \text{ or } s = s_0, \quad \varphi_0 \le \varphi \le \varphi_1 \tag{17}$$

If we wish to consider a complete shell of revolution, the kinematic and physical compatibility should be satisfied at the common meridian with $s = 0, 2\pi R_0$ in addition to the external boundary conditions. The kinematic compatibility conditions include the continuity of displacements. The physical compatibility conditions can only be the five continuous conditions for the generalized stress resultants. To consider complete revolute shells characterized by $s_0 = 2\pi R_0$, it is necessary to implement the kinematic and physical compatibility conditions between the two meridians with $s = 0$ and with $s_0 = 2\pi R_0$:

Kinematic compatibility conditions

$$\begin{aligned} &u_\varphi(\varphi,0,t) = u_\varphi(\varphi,s_0,t), u_s(\varphi,0,t) = u_s(\varphi,s_0,t), w(\varphi,0,t) = w(\varphi,s_0,t), \\ &\beta_\varphi(\varphi,0,t) = \beta_\varphi(\varphi,s_0,t), \beta_s(\varphi,0,t) = \beta_s(\varphi,s_0,t) \end{aligned} \qquad \varphi_0 \le \varphi \le \varphi_1 \tag{18}$$

Physical compatibility conditions

$$\begin{aligned} &N_s(\varphi,0,t) = N_s(\varphi,s_0,t), N_{\varphi s}(\varphi,0,t) = N_{\varphi s}(\varphi,s_0,t), T_s(\varphi,0,t) = T_s(\varphi,s_0,t), \\ &M_s(\varphi,0,t) = M_s(\varphi,s_0,t), M_{\varphi s}(\varphi,0,t) = M_{\varphi s}(\varphi,s_0,t) \end{aligned} \qquad \varphi_0 \le \varphi \le \varphi_1 \tag{19}$$

3. Generalized Differential Quadrature Method Review

The Generalized Differential Quadrature method will be used to discretize the derivatives in the governing equations in terms of displacements and the boundary and compatibility conditions.

The essence of GDQ method is that the *n*-th order derivative of a smooth one-dimensional function $f(x)$ defined over an interval $[0, L]$ at the *i*-th point of abscissa x_i, can be approximated as:

$$\left.\frac{d^n f(x)}{dx^n}\right|_{x=x_i} = \sum_{j=1}^{N} \varsigma_{ij}^{(n)} f(x_j), \quad i = 1, 2, ..., N \tag{20}$$

ACCEPTED MANUSCRIPT

where $\varsigma_{ij}^{(n)}$ are the weighting coefficients at the *i-th* point calculated for the *j-th* sampling point of the domain. In equation (20) N is the total number of the sampling points of the grid distribution and $f(x_j)$ is the value of the function at the *j-th* point.

Some simple recursive formulas are available for calculating *n*-th order derivative weighting coefficients $\varsigma_{ij}^{(n)}$ by means of Lagrange polynomial interpolation functions (Shu, 2000). The weighting coefficients for the first order derivative are:

$$\varsigma_{ij}^{(1)} = \frac{\mathbf{L}^{(1)}(x_i)}{(x_i - x_j)\mathbf{L}^{(1)}(x_j)}, \quad i, j = 1, 2, ..., N, \quad i \neq j \tag{21}$$

$$\varsigma_{ii}^{(1)} = -\sum_{j=1, j\neq i}^{N} \varsigma_{ij}^{(1)}, \quad i, j = 1, 2, ..., N, \quad i = j \tag{22}$$

In equation (21) the first derivative of Lagrange interpolating polynomials at each point x_k, $k = 1, 2, ..., N$, is:

$$\mathbf{L}^{(1)}(x_k) = \prod_{l=1, l\neq k}^{N} (x_k - x_l), \quad k = 1, 2, ..., N \tag{23}$$

For higher order derivatives ($n = 2, 3, ..., N-1$), one gets iteratively:

$$\varsigma_{ij}^{(n)} = n\left(\varsigma_{ii}^{(n-1)}\varsigma_{ij}^{(1)} - \frac{\varsigma_{ij}^{(n-1)}}{x_i - x_j}\right), \quad i, j = 1, 2, ..., N, \quad i \neq j \tag{24}$$

$$\varsigma_{ii}^{(n)} = -\sum_{j=1, j\neq i}^{N} \varsigma_{ij}^{(n)}, \quad i, j = 1, 2, ..., N, \quad i = j \tag{25}$$

From the above equations that the weighting coefficients of the second and higher order derivatives can be determined from those of the first order derivative. Furthermore, it is interesting to note that the preceding coefficients $\varsigma_{ij}^{(n)}$ are dependent on the derivative order n, on the grid point distribution x_j, $j = 1, 2, ..., N$, and on the specific point x_i, where the derivative is computed. It is worth noting that, this set of expressions for the determination of the weighting coefficients is so compact and simple that it is very easy to implement them in formulating and programming because of the recurrence feature.

Throughout the paper, the Chebyshev-Gauss-Lobatto (C-G-L) grid distribution is assumed, for which the co-ordinates of grid points (φ_i, s_j) along the reference surface are:

$$\begin{aligned} \varphi_i &= \left(1 - \cos\left(\frac{i-1}{N-1}\pi\right)\right)\frac{(\varphi_1 - \varphi_0)}{2} + \varphi_0, \quad i = 1, 2, ..., N, \quad \text{for } \varphi \in \left[\varphi_0, \varphi_1\right] \\ s_j &= \left(1 - \cos\left(\frac{j-1}{M-1}\pi\right)\right)\frac{s_0}{2}, \quad j = 1, 2, ..., M, \quad \text{for } s \in \left[0, s_0\right] \ \ (\text{with } s \le \vartheta R_0) \end{aligned} \tag{26}$$

ACCEPTED MANUSCRIPT

where N, M are the total number of sampling points used to discretize the domain in φ and s directions, respectively, of the double curved shell (Fig. 6). It has been proven that for the Lagrange interpolating polynomials, the Chebyshev-Gauss-Lobatto sampling point rule guarantees convergence and efficiency to the GDQ technique (Tornabene, 2007; Tornabene and Viola, 2007, 2008).

4. Discrete Gorverning Equations and Numerical Implementation

This section analyses the free vibration of functionally graded shells. Using the method of separation of variables, it is possible to seek solutions that are harmonic in time and whose frequency is ω. The displacements and the rotations can be written as follows:

$$\begin{aligned} u_\varphi(\varphi,s,t) &= U^\varphi(\varphi,s)e^{i\omega t} \\ u_s(\varphi,s,t) &= U^s(\varphi,s)e^{i\omega t} \\ w(\varphi,s,t) &= W(\varphi,s)e^{i\omega t} \\ \beta_\varphi(\varphi,s,t) &= B^\varphi(\varphi,s)e^{i\omega t} \\ \beta_s(\varphi,s,t) &= B^s(\varphi,s)e^{i\omega t} \end{aligned} \tag{27}$$

where the vibration spatial amplitude values $U^\varphi, U^s, W, B^\varphi, B^s$ fulfil the fundamental differential system.

The GDQ procedure allows writing of the equations of motion in discrete form, transforming each space derivative into a weighted sum of node values of dependent variables. Each approximate equation is valid in a single sampling point. The governing equations can be discretized and for the domain points, $i = 2,3,...,N-1$, $j = 2,3,...,M-1$ we have:

1) Translational equilibrium along the meridian direction φ

$$\begin{aligned} &\frac{A_{11}}{R_{\varphi i}^2}\sum_{k=1}^{N}\varsigma_{ik}^{\varphi(2)}U_{kj}^\varphi + A_{11}\left(\frac{\cos\varphi_i}{R_{\varphi i}R_{0i}} - \frac{1}{R_{\varphi i}^3}\left.\frac{dR_\varphi}{d\varphi}\right|_i\right)\sum_{k=1}^{N}\varsigma_{ik}^{\varphi(1)}U_{kj}^\varphi + A_{66}\sum_{m=1}^{M}\varsigma_{jm}^{s(2)}U_{im}^\varphi - \left(\frac{A_{12}\sin\varphi_i}{R_{\varphi i}R_{0i}} + \frac{A_{11}\cos^2\varphi_i}{R_{0i}^2} + \kappa\frac{A_{66}}{R_{\varphi i}^2}\right)U_{ij}^\varphi + \\ &-\left(\frac{A_{11}\cos\varphi_i}{R_{0i}} + \frac{A_{66}\cos\varphi_i}{R_{0i}}\right)\sum_{m=1}^{M}\varsigma_{jm}^{s(1)}U_{im}^s + \left(\frac{A_{12}}{R_{\varphi i}} + \frac{A_{66}}{R_{\varphi i}}\right)\sum_{k=1}^{N}\varsigma_{ik}^{\varphi(1)}\sum_{m=1}^{M}\varsigma_{jm}^{s(1)}U_{km}^s + \left(\frac{A_{11}}{R_{\varphi i}^2} + \frac{A_{12}\sin\varphi_i}{R_{\varphi i}R_{0i}} + \kappa\frac{A_{66}}{R_{\varphi i}^2}\right)\sum_{k=1}^{N}\varsigma_{ik}^{\varphi(1)}W_{kj} + \\ &+\left(A_{11}\left(\frac{\cos\varphi_i}{R_{\varphi i}R_{0i}} - \frac{1}{R_{\varphi i}^3}\left.\frac{dR_\varphi}{d\varphi}\right|_i\right) - \frac{A_{11}\sin\varphi_i\cos\varphi_i}{R_{0i}^2}\right)W_{ij} + \frac{B_{11}}{R_{\varphi i}^2}\sum_{k=1}^{N}\varsigma_{ik}^{\varphi(2)}B_{kj}^\varphi + B_{11}\left(\frac{\cos\varphi_i}{R_{\varphi i}R_{0i}} - \frac{1}{R_{\varphi i}^3}\left.\frac{dR_\varphi}{d\varphi}\right|_i\right)\sum_{k=1}^{N}\varsigma_{ik}^{\varphi(1)}B_{kj}^\varphi + \\ &+B_{66}\sum_{m=1}^{M}\varsigma_{jm}^{s(2)}B_{im}^\varphi - \left(\frac{B_{12}\sin\varphi_i}{R_{\varphi i}R_{0i}} + \frac{B_{11}\cos^2\varphi_i}{R_{0i}^2} - \kappa\frac{A_{66}}{R_{\varphi i}}\right)B_{ij}^\varphi - \left(\frac{B_{11}\cos\varphi_i}{R_{0i}} + \frac{B_{66}\cos\varphi_i}{R_{0i}}\right)\sum_{m=1}^{M}\varsigma_{jm}^{s(1)}B_{im}^s + \\ &+\left(\frac{B_{12}}{R_{\varphi i}} + \frac{B_{66}}{R_{\varphi i}}\right)\sum_{k=1}^{N}\varsigma_{ik}^{\varphi(1)}\sum_{m=1}^{M}\varsigma_{jm}^{s(1)}B_{km}^s = -\omega^2\left(I_0U_{ij}^\varphi + I_1B_{ij}^\varphi\right) \end{aligned} \tag{28}$$

ACCEPTED MANUSCRIPT

2) Translational equilibrium along the circumferential direction s

$$\left(\frac{A_{11}\cos\varphi_i}{R_{0i}}+\frac{A_{66}\cos\varphi_i}{R_{0i}}\right)\sum_{m=1}^{M}\varsigma_{jm}^{s(1)}U_{im}^{\varphi}+\left(\frac{A_{12}}{R_{\varphi i}}+\frac{A_{66}}{R_{\varphi i}}\right)\sum_{k=1}^{N}\varsigma_{ik}^{\varphi(1)}\sum_{m=1}^{M}\varsigma_{jm}^{s(1)}U_{km}^{\varphi}+\frac{A_{66}}{R_{\varphi i}^2}\sum_{k=1}^{N}\varsigma_{ik}^{\varphi(2)}U_{kj}^{s}+A_{66}\left(\frac{\cos\varphi_i}{R_{\varphi i}R_{0i}}-\frac{1}{R_{\varphi i}^3}\frac{dR_{\varphi}}{d\varphi}\bigg|_i\right)\sum_{k=1}^{N}\varsigma_{ik}^{\varphi(1)}U_{kj}^{s}+$$

$$+A_{11}\sum_{m=1}^{M}\varsigma_{jm}^{s(2)}U_{im}^{s}-\left(A_{66}\left(\frac{\cos^2\varphi_i}{R_{0i}^2}-\frac{\sin\varphi_i}{R_{\varphi i}R_{0i}}\right)+\kappa\frac{A_{66}\sin^2\varphi_i}{R_{0i}^2}\right)U_{ij}^{s}+\left(\frac{A_{12}}{R_{\varphi i}}+\frac{A_{11}\sin\varphi_i}{R_{0i}}+\kappa\frac{A_{66}\sin\varphi_i}{R_{0i}}\right)\sum_{m=1}^{M}\varsigma_{jm}^{s(1)}W_{im}+$$

$$+\left(\frac{B_{11}\cos\varphi_i}{R_{0i}}+\frac{B_{66}\cos\varphi_i}{R_{0i}}\right)\sum_{m=1}^{M}\varsigma_{jm}^{s(1)}B_{im}^{\varphi}+\left(\frac{B_{12}}{R_{\varphi i}}+\frac{B_{66}}{R_{\varphi i}}\right)\sum_{k=1}^{N}\varsigma_{ik}^{\varphi(1)}\sum_{m=1}^{M}\varsigma_{jm}^{s(1)}B_{km}^{\varphi}+\frac{B_{66}}{R_{\varphi i}^2}\sum_{k=1}^{N}\varsigma_{ik}^{\varphi(2)}B_{kj}^{s}+B_{66}\left(\frac{\cos\varphi_i}{R_{\varphi i}R_{0i}}-\frac{1}{R_{\varphi i}^3}\frac{dR_{\varphi}}{d\varphi}\bigg|_i\right)\sum_{k=1}^{N}\varsigma_{ik}^{\varphi(1)}B_{kj}^{s}+$$

$$+B_{11}\sum_{m=1}^{M}\varsigma_{jm}^{s(2)}B_{im}^{s}-\left(B_{66}\left(\frac{\cos^2\varphi_i}{R_{0i}^2}-\frac{\sin\varphi_i}{R_{\varphi i}R_{0i}}\right)-\kappa\frac{A_{66}\sin\varphi_i}{R_{0i}}\right)B_{ij}^{s}=-\omega^2\left(I_0U_{ij}^{s}+I_1B_{ij}^{s}\right)\tag{29}$$

3) Translational equilibrium along the normal direction ζ

$$-\left(\frac{A_{11}}{R_{\varphi i}^2}+\frac{A_{12}\sin\varphi_i}{R_{\varphi i}R_{0i}}+\kappa\frac{A_{66}}{R_{\varphi i}^2}\right)\sum_{k=1}^{N}\varsigma_{ik}^{\varphi(1)}U_{kj}^{\varphi}-\left(\frac{A_{12}\cos\varphi_i}{R_{\varphi i}R_{0i}}+\frac{A_{66}\sin\varphi_i\cos\varphi_i}{R_{0i}^2}+\kappa A_{66}\left(\frac{\cos\varphi_i}{R_{\varphi i}R_{0i}}-\frac{1}{R_{\varphi i}^3}\frac{dR_{\varphi}}{d\varphi}\bigg|_i\right)\right)U_{ij}^{\varphi}+$$

$$-\left(\frac{A_{12}}{R_{\varphi i}}+\frac{A_{11}\sin\varphi_i}{R_{0i}}+\kappa\frac{A_{66}\sin\varphi_i}{R_{0i}}\right)\sum_{m=1}^{M}\varsigma_{jm}^{s(1)}U_{im}^{s}+\kappa\frac{A_{66}}{R_{\varphi i}^2}\sum_{k=1}^{N}\varsigma_{ik}^{\varphi(2)}W_{kj}+\kappa A_{66}\left(\frac{\cos\varphi_i}{R_{\varphi i}R_{0i}}-\frac{1}{R_{\varphi i}^3}\frac{dR_{\varphi}}{d\varphi}\bigg|_i\right)\sum_{k=1}^{N}\varsigma_{ik}^{\varphi(1)}W_{kj}+$$

$$+\kappa A_{66}\sum_{m=1}^{M}\varsigma_{jm}^{s(2)}W_{im}-\left(\frac{A_{11}}{R_{\varphi i}^2}+\frac{2A_{12}\sin\varphi_i}{R_{\varphi i}R_{0i}}+\frac{A_{11}\sin^2\varphi_i}{R_{0i}^2}\right)W_{ij}-\left(\frac{B_{11}}{R_{\varphi i}^2}+\frac{B_{12}\sin\varphi_i}{R_{\varphi i}R_{0i}}-\kappa\frac{A_{66}}{R_{\varphi i}}\right)\sum_{k=1}^{N}\varsigma_{ik}^{\varphi(1)}B_{kj}^{\varphi}+$$

$$-\left(\frac{B_{12}\cos\varphi_i}{R_{\varphi i}R_{0i}}+\frac{B_{11}\sin\varphi_i\cos\varphi_i}{R_{0i}^2}-\kappa\frac{A_{66}\cos\varphi_i}{R_{0i}}\right)B_{ij}^{\varphi}-\left(\frac{B_{12}}{R_{\varphi i}}+\frac{B_{11}\sin\varphi_i}{R_{0i}}-\kappa A_{66}\right)\sum_{m=1}^{M}\varsigma_{jm}^{s(1)}B_{im}^{s}=-\omega^2I_0W_{ij}\tag{30}$$

4) Rotational equilibrium about the circumferential direction s

$$\frac{B_{11}}{R_{\varphi i}^2}\sum_{k=1}^{N}\varsigma_{ik}^{\varphi(2)}U_{kj}^{\varphi}+B_{11}\left(\frac{\cos\varphi_i}{R_{\varphi i}R_{0i}}-\frac{1}{R_{\varphi i}^3}\frac{dR_{\varphi}}{d\varphi}\bigg|_i\right)\sum_{k=1}^{N}\varsigma_{ik}^{\varphi(1)}U_{kj}^{\varphi}+B_{66}\sum_{m=1}^{M}\varsigma_{jm}^{s(2)}U_{im}^{\varphi}-\left(\frac{B_{12}\sin\varphi_i}{R_{\varphi i}R_{0i}}+\frac{B_{11}\cos^2\varphi_i}{R_{0i}^2}-\kappa\frac{A_{66}}{R_{\varphi i}}\right)U_{ij}^{\varphi}+$$

$$-\left(\frac{B_{11}\cos\varphi_i}{R_{0i}}+\frac{B_{66}\cos\varphi_i}{R_{0i}}\right)\sum_{m=1}^{M}\varsigma_{jm}^{s(1)}U_{im}^{s}+\left(\frac{B_{12}}{R_{\varphi i}}+\frac{B_{66}}{R_{\varphi i}}\right)\sum_{k=1}^{N}\varsigma_{ik}^{\varphi(1)}\sum_{m=1}^{M}\varsigma_{jm}^{s(1)}U_{km}^{s}+\left(\frac{B_{11}}{R_{\varphi i}^2}+\frac{B_{12}\sin\varphi_i}{R_{\varphi i}R_{0i}}-\kappa\frac{A_{66}}{R_{\varphi i}}\right)\sum_{k=1}^{N}\varsigma_{ik}^{\varphi(1)}W_{kj}+$$

$$+\left(B_{11}\left(\frac{\cos\varphi_i}{R_{\varphi i}R_{0i}}-\frac{1}{R_{\varphi i}^3}\frac{dR_{\varphi}}{d\varphi}\bigg|_i\right)-\frac{B_{11}\sin\varphi_i\cos\varphi_i}{R_{0i}^2}\right)W_{ij}+\frac{D_{11}}{R_{\varphi i}^2}\sum_{k=1}^{N}\varsigma_{ik}^{\varphi(2)}B_{kj}^{\varphi}+D_{11}\left(\frac{\cos\varphi_i}{R_{\varphi i}R_{0i}}-\frac{1}{R_{\varphi i}^3}\frac{dR_{\varphi}}{d\varphi}\bigg|_i\right)\sum_{k=1}^{N}\varsigma_{ik}^{\varphi(1)}B_{kj}^{\varphi}+$$

$$+D_{66}\sum_{m=1}^{M}\varsigma_{jm}^{s(2)}B_{im}^{\varphi}-\left(\frac{D_{12}\sin\varphi_i}{R_{\varphi i}R_{0i}}+\frac{D_{11}\cos^2\varphi_i}{R_{0i}^2}+\kappa A_{66}\right)B_{ij}^{\varphi}-\left(\frac{D_{11}\cos\varphi_i}{R_{0i}}+\frac{D_{66}\cos\varphi_i}{R_{0i}}\right)\sum_{m=1}^{M}\varsigma_{jm}^{s(1)}B_{im}^{s}+$$

$$+\left(\frac{D_{12}}{R_{\varphi i}}+\frac{D_{66}}{R_{\varphi i}}\right)\sum_{k=1}^{N}\varsigma_{ik}^{\varphi(1)}\sum_{m=1}^{M}\varsigma_{jm}^{s(1)}B_{km}^{s}=-\omega^2\left(I_1U_{ij}^{\varphi}+I_2B_{ij}^{\varphi}\right)\tag{31}$$

ACCEPTED MANUSCRIPT

5) Rotational equilibrium about the meridian direction φ

$$\left(\frac{B_{11}\cos\varphi_i}{R_{0i}}+\frac{B_{66}\cos\varphi_i}{R_{0i}}\right)\sum_{m=1}^{M}\varsigma_{jm}^{s(1)}U_{im}^{\varphi}+\left(\frac{B_{12}}{R_{\varphi i}}+\frac{B_{66}}{R_{\varphi i}}\right)\sum_{k=1}^{N}\varsigma_{ik}^{\varphi(1)}\sum_{m=1}^{M}\varsigma_{jm}^{s(1)}U_{km}^{\varphi}+\frac{B_{66}}{R_{\varphi i}^{2}}\sum_{k=1}^{N}\varsigma_{ik}^{\varphi(2)}U_{kj}^{s}+B_{66}\left(\frac{\cos\varphi_i}{R_{\varphi i}R_{0i}}-\frac{1}{R_{\varphi i}^{3}}\frac{dR_{\varphi}}{d\varphi}\bigg|_{i}\right)\sum_{k=1}^{N}\varsigma_{ik}^{\varphi(1)}U_{kj}^{s}+$$

$$+B_{11}\sum_{m=1}^{M}\varsigma_{jm}^{s(2)}U_{im}^{s}-\left(B_{66}\left(\frac{\cos^{2}\varphi_i}{R_{0i}^{2}}-\frac{\sin\varphi_i}{R_{\varphi i}R_{0i}}\right)-\kappa\frac{A_{66}\sin\varphi_i}{R_{0i}}\right)U_{ij}^{s}+\left(\frac{B_{12}}{R_{\varphi i}}+\frac{B_{11}\sin\varphi_i}{R_{0i}}-\kappa A_{66}\right)\sum_{m=1}^{M}\varsigma_{jm}^{s(1)}W_{im}+$$

$$+\left(\frac{D_{11}\cos\varphi_i}{R_{0i}}+\frac{D_{66}\cos\varphi_i}{R_{0i}}\right)\sum_{m=1}^{M}\varsigma_{jm}^{s(1)}B_{im}^{\varphi}+\left(\frac{D_{12}}{R_{\varphi i}}+\frac{D_{66}}{R_{\varphi i}}\right)\sum_{k=1}^{N}\varsigma_{ik}^{\varphi(1)}\sum_{m=1}^{M}\varsigma_{jm}^{s(1)}B_{km}^{\varphi}+\frac{D_{66}}{R_{\varphi i}^{2}}\sum_{k=1}^{N}\varsigma_{ik}^{\varphi(2)}B_{kj}^{s}+D_{66}\left(\frac{\cos\varphi_i}{R_{\varphi i}R_{0i}}-\frac{1}{R_{\varphi i}^{3}}\frac{dR_{\varphi}}{d\varphi}\bigg|_{i}\right)\sum_{k=1}^{N}\varsigma_{ik}^{\varphi(1)}B_{kj}^{s}+$$

$$+D_{11}\sum_{m=1}^{M}\varsigma_{jm}^{s(2)}B_{im}^{s}-\left(D_{66}\left(\frac{\cos^{2}\varphi_i}{R_{0i}^{2}}-\frac{\sin\varphi_i}{R_{\varphi i}R_{0i}}\right)+\kappa A_{66}\right)B_{ij}^{s}=-\omega^{2}\left(I_1U_{ij}^{s}+I_2B_{ij}^{s}\right)\tag{32}$$

In equations (28)-(32), $\varsigma_{ik}^{\varphi(1)}$, $\varsigma_{jm}^{s(1)}$, $\varsigma_{ik}^{\varphi(2)}$ and $\varsigma_{jm}^{s(2)}$ are the weighting coefficients of the first and second derivatives in φ and s directions, respectively. Furthermore, N and M are the total number of grid points in φ and s directions.

Applying the GDQ methodology, the discretized forms of the boundary and compatibility conditions are given as follows:

Clamped edge boundary condition (C)

$$\begin{aligned}&U_{aj}^{\varphi}=U_{aj}^{s}=W_{aj}=B_{aj}^{\varphi}=B_{aj}^{s}=0 \quad \text{for } a=1,N \text{ and } j=1,2,...,M\\&U_{ib}^{\varphi}=U_{ib}^{s}=W_{ib}=B_{ib}^{\varphi}=B_{ib}^{s}=0 \quad \text{for } b=1,M \text{ and } i=1,2,...,N\end{aligned}\tag{33}$$

Simply supported edge boundary condition (S)

$$\begin{cases}U_{aj}^{\varphi}=U_{aj}^{s}=W_{aj}=B_{aj}^{s}=0\\ \dfrac{B_{11}}{R_{\varphi a}}\displaystyle\sum_{k=1}^{N}\varsigma_{ak}^{\varphi(1)}U_{kj}^{\varphi}+\frac{B_{12}\cos\varphi_a}{R_{0a}}U_{aj}^{\varphi}+B_{12}\sum_{m=1}^{M}\varsigma_{jm}^{s(1)}U_{am}^{s}+\\ +\left(\dfrac{B_{11}}{R_{\varphi a}}+\dfrac{B_{12}\sin\varphi_a}{R_{0a}}\right)W_{aj}+\dfrac{D_{11}}{R_{\varphi a}}\displaystyle\sum_{k=1}^{N}\varsigma_{ak}^{\varphi(1)}B_{kj}^{\varphi}+ \qquad \text{for } a=1,N \text{ and } j=1,2,...,M\\ +\dfrac{D_{12}\cos\varphi_a}{R_{0a}}B_{aj}^{\varphi}+D_{12}\displaystyle\sum_{m=1}^{M}\varsigma_{jm}^{s(1)}B_{am}^{s}=0\end{cases}\tag{34}$$

$$\begin{cases}U_{ib}^{\varphi}=U_{ib}^{s}=W_{ib}=B_{ib}^{\varphi}=0\\ \dfrac{B_{12}}{R_{\varphi i}}\displaystyle\sum_{k=1}^{N}\varsigma_{ik}^{\varphi(1)}U_{kb}^{\varphi}+\frac{B_{11}\cos\varphi_i}{R_{0i}}U_{ib}^{\varphi}+B_{11}\sum_{m=1}^{M}\varsigma_{bm}^{s(1)}U_{im}^{s}+\\ +\left(\dfrac{B_{12}}{R_{\varphi i}}+\dfrac{B_{11}\sin\varphi_i}{R_{0i}}\right)W_{ib}+\dfrac{D_{12}}{R_{\varphi i}}\displaystyle\sum_{k=1}^{N}\varsigma_{ik}^{\varphi(1)}B_{kb}^{\varphi}+ \qquad \text{for } b=1,M \text{ and } i=1,2,...,N\\ +\dfrac{D_{11}\cos\varphi_i}{R_{0i}}B_{ib}^{\varphi}+D_{11}\displaystyle\sum_{m=1}^{M}\varsigma_{bm}^{s(1)}B_{im}^{s}=0\end{cases}$$

ACCEPTED MANUSCRIPT

Free edge boundary condition (F)

$$\begin{cases}
\dfrac{A_{11}}{R_{\varphi a}}\sum_{k=1}^{N}\varsigma_{ak}^{\varphi(1)}U_{kj}^{\varphi}+\dfrac{A_{12}\cos\varphi_a}{R_{0a}}U_{aj}^{\varphi}+A_{12}\sum_{m=1}^{M}\varsigma_{jm}^{s(1)}U_{am}^{s}+\left(\dfrac{A_{11}}{R_{\varphi a}}+\dfrac{A_{12}\sin\varphi_a}{R_{0a}}\right)W_{aj}+\dfrac{B_{11}}{R_{\varphi a}}\sum_{k=1}^{N}\varsigma_{ak}^{\varphi(1)}B_{kj}^{\varphi}+\dfrac{B_{12}\cos\varphi_a}{R_{0a}}B_{aj}^{\varphi}+B_{12}\sum_{m=1}^{M}\varsigma_{jm}^{s(1)}B_{am}^{s}=0\\
A_{66}\sum_{m=1}^{M}\varsigma_{jm}^{s(1)}U_{am}^{\varphi}+\dfrac{A_{66}}{R_{\varphi a}}\sum_{k=1}^{N}\varsigma_{ak}^{\varphi(1)}U_{kj}^{s}-\dfrac{A_{66}\cos\varphi_a}{R_{0a}}U_{aj}^{s}+B_{66}\sum_{m=1}^{M}\varsigma_{jm}^{s(1)}B_{am}^{\varphi}+\dfrac{B_{66}}{R_{\varphi a}}\sum_{k=1}^{N}\varsigma_{ak}^{\varphi(1)}B_{kj}^{s}-\dfrac{B_{66}\cos\varphi_a}{R_{0a}}B_{aj}^{s}=0\\
-\kappa\dfrac{A_{66}}{R_{\varphi a}}U_{aj}^{\varphi}+\kappa\dfrac{A_{66}}{R_{\varphi a}}\sum_{k=1}^{N}\varsigma_{ak}^{\varphi(1)}W_{kj}+\kappa A_{66}B_{aj}^{\varphi}+\kappa A_{66}B_{aj}^{s}=0\\
\dfrac{B_{11}}{R_{\varphi a}}\sum_{k=1}^{N}\varsigma_{ak}^{\varphi(1)}U_{kj}^{\varphi}+\dfrac{B_{12}\cos\varphi_a}{R_{0a}}U_{aj}^{\varphi}+B_{12}\sum_{m=1}^{M}\varsigma_{jm}^{s(1)}U_{am}^{s}+\left(\dfrac{B_{11}}{R_{\varphi a}}+\dfrac{B_{12}\sin\varphi_a}{R_{0a}}\right)W_{aj}+\dfrac{D_{11}}{R_{\varphi a}}\sum_{k=1}^{N}\varsigma_{ak}^{\varphi(1)}B_{kj}^{\varphi}+\dfrac{D_{12}\cos\varphi_a}{R_{0a}}B_{aj}^{\varphi}+D_{12}\sum_{m=1}^{M}\varsigma_{jm}^{s(1)}B_{am}^{s}=0\\
B_{66}\sum_{m=1}^{M}\varsigma_{jm}^{s(1)}U_{am}^{\varphi}+\dfrac{B_{66}}{R_{\varphi a}}\sum_{k=1}^{N}\varsigma_{ak}^{\varphi(1)}U_{kj}^{s}-\dfrac{B_{66}\cos\varphi_a}{R_{0a}}U_{aj}^{s}+D_{66}\sum_{m=1}^{M}\varsigma_{jm}^{s(1)}B_{am}^{\varphi}+\dfrac{D_{66}}{R_{\varphi a}}\sum_{k=1}^{N}\varsigma_{ak}^{\varphi(1)}B_{kj}^{s}-\dfrac{D_{66}\cos\varphi_a}{R_{0a}}B_{aj}^{s}=0
\end{cases}\qquad(35)$$

$$\text{for } a=1,N \text{ and } j=1,2,...,M$$

$$\begin{cases}
A_{66}\sum_{m=1}^{M}\varsigma_{bm}^{s(1)}U_{im}^{\varphi}+\dfrac{A_{66}}{R_{\varphi i}}\sum_{k=1}^{N}\varsigma_{ik}^{\varphi(1)}U_{kb}^{s}-\dfrac{A_{66}\cos\varphi_i}{R_{0i}}U_{ib}^{s}+B_{66}\sum_{m=1}^{M}\varsigma_{bm}^{s(1)}B_{im}^{\varphi}+\dfrac{B_{66}}{R_{\varphi i}}\sum_{k=1}^{N}\varsigma_{ik}^{\varphi(1)}B_{kb}^{s}-\dfrac{B_{66}\cos\varphi_i}{R_{0i}}B_{ib}^{s}=0\\
\dfrac{A_{12}}{R_{\varphi i}}\sum_{k=1}^{N}\varsigma_{ik}^{\varphi(1)}U_{kb}^{\varphi}+\dfrac{A_{11}\cos\varphi_i}{R_{0i}}U_{ib}^{\varphi}+A_{11}\sum_{m=1}^{M}\varsigma_{bm}^{s(1)}U_{im}^{s}+\left(\dfrac{A_{12}}{R_{\varphi i}}+\dfrac{A_{11}\sin\varphi_i}{R_{0i}}\right)W_{ib}+\dfrac{B_{12}}{R_{\varphi i}}\sum_{k=1}^{N}\varsigma_{ik}^{\varphi(1)}B_{kb}^{\varphi}+\dfrac{B_{11}\cos\varphi_i}{R_{0i}}B_{ib}^{\varphi}+B_{11}\sum_{m=1}^{M}\varsigma_{bm}^{s(1)}B_{im}^{s}=0\\
\kappa\dfrac{A_{66}}{R_{\varphi i}}\sum_{k=1}^{N}\varsigma_{ik}^{\varphi(1)}W_{kb}+\kappa A_{66}B_{ib}^{\varphi}+\kappa A_{66}B_{ib}^{s}=0\\
B_{66}\sum_{m=1}^{M}\varsigma_{bm}^{s(1)}U_{im}^{\varphi}+\dfrac{B_{66}}{R_{\varphi i}}\sum_{k=1}^{N}\varsigma_{ik}^{\varphi(1)}U_{kb}^{s}-\dfrac{B_{66}\cos\varphi_i}{R_{0i}}U_{ib}^{s}+D_{66}\sum_{m=1}^{M}\varsigma_{bm}^{s(1)}B_{im}^{\varphi}+\dfrac{D_{66}}{R_{\varphi i}}\sum_{k=1}^{N}\varsigma_{ik}^{\varphi(1)}B_{kb}^{s}-\dfrac{D_{66}\cos\varphi_i}{R_{0i}}B_{ib}^{s}=0\\
\dfrac{B_{12}}{R_{\varphi i}}\sum_{k=1}^{N}\varsigma_{ik}^{\varphi(1)}U_{kb}^{\varphi}+\dfrac{B_{11}\cos\varphi_i}{R_{0i}}U_{ib}^{\varphi}+B_{11}\sum_{m=1}^{M}\varsigma_{bm}^{s(1)}U_{im}^{s}+\left(\dfrac{B_{12}}{R_{\varphi i}}+\dfrac{B_{11}\sin\varphi_i}{R_{0i}}\right)W_{ib}+\dfrac{D_{12}}{R_{\varphi i}}\sum_{k=1}^{N}\varsigma_{ik}^{\varphi(1)}B_{kb}^{\varphi}+\dfrac{D_{11}\cos\varphi_i}{R_{0i}}B_{ib}^{\varphi}+D_{11}\sum_{m=1}^{M}\varsigma_{bm}^{s(1)}B_{im}^{s}=0
\end{cases}\qquad(36)$$

$$\text{for } b=1,M \text{ and } i=1,2,...,N$$

Kinematic and physical compatibility conditions

$$U_{i1}^{\varphi}=U_{iM}^{\varphi},U_{i1}^{s}=U_{iM}^{s},W_{i1}=W_{iM},B_{i1}^{\varphi}=B_{iM}^{\varphi},B_{i1}^{s}=B_{iM}^{s}$$

$$\begin{cases}
A_{66}\sum_{m=1}^{M}\varsigma_{1m}^{s(1)}U_{im}^{\varphi}+\dfrac{A_{66}}{R_{\varphi i}}\sum_{k=1}^{N}\varsigma_{ik}^{\varphi(1)}U_{k1}^{s}-\dfrac{A_{66}\cos\varphi_i}{R_{0i}}U_{i1}^{s}+B_{66}\sum_{m=1}^{M}\varsigma_{1m}^{s(1)}B_{im}^{\varphi}+\dfrac{B_{66}}{R_{\varphi i}}\sum_{k=1}^{N}\varsigma_{ik}^{\varphi(1)}B_{k1}^{s}-\dfrac{B_{66}\cos\varphi_i}{R_{0i}}B_{i1}^{s}=\\
=A_{66}\sum_{m=1}^{M}\varsigma_{Mm}^{s(1)}U_{im}^{\varphi}+\dfrac{A_{66}}{R_{\varphi i}}\sum_{k=1}^{N}\varsigma_{ik}^{\varphi(1)}U_{kM}^{s}-\dfrac{A_{66}\cos\varphi_i}{R_{0i}}U_{iM}^{s}+B_{66}\sum_{m=1}^{M}\varsigma_{Mm}^{s(1)}B_{im}^{\varphi}+\dfrac{B_{66}}{R_{\varphi i}}\sum_{k=1}^{N}\varsigma_{ik}^{\varphi(1)}B_{kM}^{s}-\dfrac{B_{66}\cos\varphi_i}{R_{0i}}B_{iM}^{s}\\
\dfrac{A_{12}}{R_{\varphi i}}\sum_{k=1}^{N}\varsigma_{ik}^{\varphi(1)}U_{k1}^{\varphi}+\dfrac{A_{11}\cos\varphi_i}{R_{0i}}U_{i1}^{\varphi}+A_{11}\sum_{m=1}^{M}\varsigma_{1m}^{s(1)}U_{im}^{s}+\left(\dfrac{A_{12}}{R_{\varphi i}}+\dfrac{A_{11}\sin\varphi_i}{R_{0i}}\right)W_{i1}+\dfrac{B_{12}}{R_{\varphi i}}\sum_{k=1}^{N}\varsigma_{ik}^{\varphi(1)}B_{k1}^{\varphi}+\dfrac{B_{11}\cos\varphi_i}{R_{0i}}B_{i1}^{\varphi}+B_{11}\sum_{m=1}^{M}\varsigma_{1m}^{s(1)}B_{im}^{s}=\\
=\dfrac{A_{12}}{R_{\varphi i}}\sum_{k=1}^{N}\varsigma_{ik}^{\varphi(1)}U_{kM}^{\varphi}+\dfrac{A_{11}\cos\varphi_i}{R_{0i}}U_{iM}^{\varphi}+A_{11}\sum_{m=1}^{M}\varsigma_{Mm}^{s(1)}U_{im}^{s}+\left(\dfrac{A_{12}}{R_{\varphi i}}+\dfrac{A_{11}\sin\varphi_i}{R_{0i}}\right)W_{iM}+\dfrac{B_{12}}{R_{\varphi i}}\sum_{k=1}^{N}\varsigma_{ik}^{\varphi(1)}B_{kM}^{\varphi}+\dfrac{B_{11}\cos\varphi_i}{R_{0i}}B_{iM}^{\varphi}+B_{11}\sum_{m=1}^{M}\varsigma_{Mm}^{s(1)}B_{im}^{s}\\
\kappa\dfrac{A_{66}}{R_{\varphi i}}\sum_{k=1}^{N}\varsigma_{ik}^{\varphi(1)}W_{k1}+\kappa A_{66}B_{i1}^{\varphi}+\kappa A_{66}B_{i1}^{s}=\kappa\dfrac{A_{66}}{R_{\varphi i}}\sum_{k=1}^{N}\varsigma_{ik}^{\varphi(1)}W_{kM}+\kappa A_{66}B_{iM}^{\varphi}+\kappa A_{66}B_{iM}^{s}\\
B_{66}\sum_{m=1}^{M}\varsigma_{1m}^{s(1)}U_{im}^{\varphi}+\dfrac{B_{66}}{R_{\varphi i}}\sum_{k=1}^{N}\varsigma_{ik}^{\varphi(1)}U_{k1}^{s}-\dfrac{B_{66}\cos\varphi_i}{R_{0i}}U_{i1}^{s}+D_{66}\sum_{m=1}^{M}\varsigma_{1m}^{s(1)}B_{im}^{\varphi}+\dfrac{D_{66}}{R_{\varphi i}}\sum_{k=1}^{N}\varsigma_{ik}^{\varphi(1)}B_{k1}^{s}-\dfrac{D_{66}\cos\varphi_i}{R_{0i}}B_{i1}^{s}=\\
=B_{66}\sum_{m=1}^{M}\varsigma_{Mm}^{s(1)}U_{im}^{\varphi}+\dfrac{B_{66}}{R_{\varphi i}}\sum_{k=1}^{N}\varsigma_{ik}^{\varphi(1)}U_{kM}^{s}-\dfrac{B_{66}\cos\varphi_i}{R_{0i}}U_{iM}^{s}+D_{66}\sum_{m=1}^{M}\varsigma_{Mm}^{s(1)}B_{im}^{\varphi}+\dfrac{D_{66}}{R_{\varphi i}}\sum_{k=1}^{N}\varsigma_{ik}^{\varphi(1)}B_{kM}^{s}-\dfrac{D_{66}\cos\varphi_i}{R_{0i}}B_{iM}^{s}\\
\dfrac{B_{12}}{R_{\varphi i}}\sum_{k=1}^{N}\varsigma_{ik}^{\varphi(1)}U_{k1}^{\varphi}+\dfrac{B_{11}\cos\varphi_i}{R_{0i}}U_{i1}^{\varphi}+B_{11}\sum_{m=1}^{M}\varsigma_{1m}^{s(1)}U_{im}^{s}+\left(\dfrac{B_{12}}{R_{\varphi i}}+\dfrac{B_{11}\sin\varphi_i}{R_{0i}}\right)W_{i1}+\dfrac{D_{12}}{R_{\varphi i}}\sum_{k=1}^{N}\varsigma_{ik}^{\varphi(1)}B_{k1}^{\varphi}+\dfrac{D_{11}\cos\varphi_i}{R_{0i}}B_{i1}^{\varphi}+D_{11}\sum_{m=1}^{M}\varsigma_{1m}^{s(1)}B_{im}^{s}=\\
=\dfrac{B_{12}}{R_{\varphi i}}\sum_{k=1}^{N}\varsigma_{ik}^{\varphi(1)}U_{kM}^{\varphi}+\dfrac{B_{11}\cos\varphi_i}{R_{0i}}U_{iM}^{\varphi}+B_{11}\sum_{m=1}^{M}\varsigma_{Mm}^{s(1)}U_{im}^{s}+\left(\dfrac{B_{12}}{R_{\varphi i}}+\dfrac{B_{11}\sin\varphi_i}{R_{0i}}\right)W_{iM}+\dfrac{D_{12}}{R_{\varphi i}}\sum_{k=1}^{N}\varsigma_{ik}^{\varphi(1)}B_{kM}^{\varphi}+\dfrac{D_{11}\cos\varphi_i}{R_{0i}}B_{iM}^{\varphi}+D_{11}\sum_{m=1}^{M}\varsigma_{Mm}^{s(1)}B_{im}^{s}
\end{cases}\qquad(37)$$

$$\text{for } i=2,...,N-1$$

Thus, the whole system of differential equations has been discretized and the global assembling leads to the

ACCEPTED MANUSCRIPT

following set of linear algebraic equations:

$$\left[\begin{array}{c|c} \mathbf{K}_{bb} & \mathbf{K}_{bd} \\ \hline \mathbf{K}_{db} & \mathbf{K}_{dd} \end{array}\right]\left[\begin{array}{c} \boldsymbol{\delta}_b \\ \hline \boldsymbol{\delta}_d \end{array}\right] = \omega^2 \left[\begin{array}{c|c} \mathbf{0} & \mathbf{0} \\ \hline \mathbf{0} & \mathbf{M}_{dd} \end{array}\right]\left[\begin{array}{c} \boldsymbol{\delta}_b \\ \hline \boldsymbol{\delta}_d \end{array}\right] \tag{38}$$

In the above matrices and vectors, the partitioning is set forth by subscripts b and d, referring to the system degrees of freedom and standing for boundary and domain, respectively. In this sense, the b-equations represent the discrete boundary and compatibility conditions, which are valid only for the points lying on constrained edges of the shell; while the d-equations are the equilibrium equations, assigned on interior nodes. In order to make the computation more efficient, kinematic condensation of non-domain degrees of freedom is performed:

$$\left(\mathbf{K}_{dd} - \mathbf{K}_{db}\left(\mathbf{K}_{bb}\right)^{-1}\mathbf{K}_{bd}\right)\boldsymbol{\delta}_d = \omega^2 \mathbf{M}_{dd}\boldsymbol{\delta}_d \tag{39}$$

The natural frequencies of the structure considered can be determined by solving the standard eigenvalue problem (39). In particular, the solution procedure by means of GDQ technique has been implemented in a MATLAB code. Finally, the results in terms of frequencies are obtained using the *eigs* function of MATLAB program.

It is worth noting that, with the present approach, differing from the finite element method, no integration occurs prior to the global assembly of the linear system, and this leads to a further computational cost saving in favour of the differential quadrature technique.

5. Results and Discussion

This section introduces some results and considerations about the free vibration problem of functionally graded parabolic panels and shells of revolution. The analysis has been carried out by means of numerical procedures illustrated above.

No literature is available about the results of the GDQ solution for free vibrations of FGM shells with parabolic meridian. Several attempts to validate the present formulations have been made for the isotropic and anisotropic cases and can be found in the PhD Thesis by Tornabene (2007) and in articles by Tornabene and Viola (2007, 2008). In this work, the frequency parameters from the present formulations are in good agreement with the results presented in the literature and obtained with the finite element method.

Regarding the functionally graded materials, their two constituents are taken to be zirconia (ceramic) and aluminum (metal). Young's modulus, Poisson's ratio and mass density for the zirconia are $E_C = 168\,\text{GPa}$, $\nu_C = 0.3$, $\rho_C = 5700\,\text{Kg}/\text{m}^3$, and for the aluminum are $E_M = 70\,\text{GPa}$, $\nu_M = 0.3$, $\rho_M = 2707\,\text{Kg}/\text{m}^3$, respectively. The details regarding the geometry of the structures considered are indicated below:

ACCEPTED MANUSCRIPT

1. *Toro-parabolic panel* (C-F-C-F)/(S-F-S-F): $k=9$, $R_b=9\,\text{m}$, $h=0.4\,\text{m}$, $s_1=3\,\text{m}$, $s_0=-3\,\text{m}$, $S=2\,\text{m}$, $\vartheta_0=120°$;
2. *Parabolic panel* (C-F-F-F): $k=8$, $R_b=0\,\text{m}$, $h=0.2\,\text{m}$, $s_1=4\,\text{m}$, $s_0=1\,\text{m}$, $S=2\,\text{m}$, $\vartheta_0=120°$;
3. *Parabolic toroid* (F-C): $k=4.5$, $R_b=6\,\text{m}$, $h=0.3\,\text{m}$, $s_1=0\,\text{m}$, $s_0=-3\,\text{m}$, $S=2\,\text{m}$, $\vartheta_0=360°$;
4. *Parabolic dome* (C-F): $k=8$, $R_b=0\,\text{m}$, $h=0.2\,\text{m}$, $s_1=4\,\text{m}$, $s_0=1\,\text{m}$, $S=2\,\text{m}$, $\vartheta_0=360°$.

The geometrical boundary conditions for the shell panel are identified by the following convention. For example, the symbolism C-S-C-F indicates that the edges $\varphi=\varphi_1$, $s=s_0$, $\varphi=\varphi_0$, $s=0$ are clamped, simply supported, clamped and free, respectively (Fig. 6). For the complete shell of revolution, for example, the symbolism C-F indicates that the edges $\varphi=\varphi_1$ and $\varphi=\varphi_0$ are clamped and free, respectively. In this case, the missing boundary conditions are the kinematic and physical compatibility conditions that are applied at the same meridian for $s=0$ and $s_0=2\pi R_0$.

In Figs. 7-10, the first mode shapes for the $FGM_{1(a=1/b=0.5/c=2/p=1)}$ toro-parabolic panel (C-F-C-F), the $FGM_{1(a=1/b=1/c=3/p=1)}$ parabolic panel (C-F-F-F), the $FGM_{1(a=0/b=-0.5/c=2/p=1)}$ parabolic toroid (F-C) and the $FGM_{1(a=0.8/b=0.2/c=3/p=1)}$ parabolic dome (C-F) are illustrated. In particular, for the parabolic toroid and dome, there are some symmetrical mode shapes due to the symmetry of the problem considered in 3D space. In these cases, the symmetrical mode shapes have been summarized in one figure. The mode shapes of all the structures under discussion have been evaluated by the authors. By using the authors' MATLAB code, these mode shapes have been reconstructed in three-dimensional view by means of considering the displacement field (2) after solving the eigenvalue problem (39).

Tables 1-6 illustrate the first ten frequencies of the four structures under consideration. These tables show how by varying only the power-law index p of the volume fraction V_C it is possible to modify natural frequencies of FGM panels and shells of revolution. For the GDQ results presented in Tables 1-6, the grid distributions (26) with $N=M=21$ have been taking into account. The results are obtained using various values of the power-law exponent p (i.e. $p=0$ ceramic rich and $p=\infty$ metal rich) for the two power-law distributions $FGM_{1(a/b/c/p)}$ and $FGM_{2(a/b/c/p)}$. For each power-law distribution the same values of the three parameters a,b,c are chosen.

Tables 1-6 show that by considering the two power-law distributions $FGM_{1(a/b/c/p)}$ and $FGM_{2(a/b/c/p)}$ with the same values of the four parameters a,b,c,p the natural frequencies are different. In fact, for curved shells it is important, from the dynamic vibration point of view, to know if the top surface of the shell $\left(\zeta=h/2\right)$ is ceramic or metal rich and, inversely, if the bottom surface $\left(\zeta=-h/2\right)$ is metal or ceramic rich, respectively. Using one of the

ACCEPTED MANUSCRIPT

two power-law distributions $FGM_{1(a/b/c/p)}$ and $FGM_{2(a/b/c/p)}$ changes the dynamic behaviour of the shell structure. Furthermore, Tables 1-6 show the effect of the power-law distribution choice on the frequency parameters. It is worth noting that the difference between $FGM_{1(a/b/c/p)}$ and $FGM_{2(a/b/c/p)}$ shell frequencies increases with increasing values of the shell thickness because of the curvature of the shell. From tables 1-6 it is evident that functionally graded shell and panel structures behave like the corresponding homogeneous structures ($p=0$), for $p=0.6$ and $p=1$. A similar behaviour was pointed out before by Abrate (2006) for the functionally graded plate.

The influence of the index p on the vibration frequencies is also shown in Figs. 11-16. As it can be seen from figures, natural frequencies of FGM panels and shells of revolution often present an intermediate value between the natural frequencies of the limit cases of homogeneous shells of zirconia ($p=0$) and of aluminium ($p=\infty$), as expected. However, natural frequencies sometimes exceed the limit cases, as evident in Figs. 11, 15 and 16. This fact can depend on various parameters, such as the geometry of the shell, the boundary conditions, the power-law distribution profile, etc. In particular, for specific values of the four parameters a,b,c,p it is possible to exceed or approach the ceramic limit case as shown in Figs. 11-16, even if the ceramic content is not high. Increasing the values of the parameter index p up to infinity reduces the ceramic content and at the same time increases the metal percentage. Therefore, it is possible to obtain dynamic characteristics similar or better than the isotropic ceramic limit case by choosing suitable values of the four parameters a,b,c,p.

Each of Figs. 11-16 is divided into two parts. On the left, figures (a) show the first four frequencies versus the power-law index p obtained using the $FGM_{1(a/b/c/p)}$ distribution, while on the right, figures (b) illustrate the first four frequencies versus the power-law index p obtained using the $FGM_{2(a/b/c/p)}$ distribution.

Fig. 11 shows the first four natural frequencies of the toro-parabolic panel (C-F-C-F) versus the power-law index p for various values of the parameter b, when $a=1, c=2$. Figs. 11(a) illustrate the variation of the first four frequencies obtained using the $FGM_{1(a=1/0\le b\le 1/c=2/p)}$ distribution, while in figures 11(b) the first four frequencies for the $FGM_{2(a=1/0\le b\le 1/c=2/p)}$ distribution are reported. It is interesting to note that, for the structures under consideration, frequencies attain a minimum value for a shell made only of metal, due to the fact that aluminium has a much smaller Young's modulus than zirconia. In particular, it is evident that in Fig. 11 for low values of the parameter b most frequencies exhibit a fastly decreasing behaviour from the ceramic limit case ($p=0$) varying the power-law index from $p=0$ to $p\approx 1$. For values of p greater than unity frequencies increase until a maximum value. After this maximum, frequencies slowly decrease by increasing the power-law exponent p and tend to the metal limit

ACCEPTED MANUSCRIPT

case ($p=\infty$). This is expected because the more p increases the more the ceramic content is low and the FGM shell approaches the case of the fully metal shell. Otherwise, in Fig. 11 for values of the parameter b approaching the unity the frequency curves present a fastly rising behaviour up to a maximum value by increasing the power-law index p and exceed the ceramic limit case. After this maximum, frequencies gradually decrease.

In the same way, by setting different values of parameters a,c , Figs. 12-13 ($a=1,c=1$) and 14 ($a=0,c=2$) show the influence of the parameter b on the dynamic vibration of the toro-parabolic panel (S-F-S-F), of the parabolic panel (C-F-F-F) and of the parabolic toroid (F-C), respectively. In Figs. 12 and 13 the parameter b varies from 0 to 1, as in Fig. 11, while in Fig. 14 from -1 to 0. Moreover, the influence of the parameter a on the dynamic vibration of parabolic dome (C-F) is investigated in Fig. 15 by considering $b=0.2,c=3$. In this case the parameter a varies from 0.2 to 1.2. It can be noted that in Fig. 15, for low values of the parameter a, most frequencies exhibit a fastly decreasing behaviour from the ceramic limit case ($p=0$) varying the power-law index from $p=0$ to $p\approx 1$, while for values of p greater than unity frequencies increase until a maximum value. After this maximum, frequencies slowly decrease by increasing the power-law exponent p and tend to the metal limit case ($p=\infty$). Otherwise, approaching the value $a=1.2$ the frequency curves do not present a knee as previously described, but present a fast rising behaviour up to a maximum value by increasing the power-law index p and exceed the ceramic limit case. After this maximum, frequencies gradually decrease. This behaviour depends on the type of vibration mode. It is worth noting that some frequencies do not present a knee or a maximum value as described above, but decrease gradually from the ceramic limit case ($p=0$) to the metal limit case ($p=\infty$) by increasing the power-law exponent p. In particular, the types of vibration mode that can present a monotone gradually decrease of frequency are torsional, bending and axisymmetric mode shapes, while the circumferential and radial mode shapes are characterized by a knee or a maximum value, as it can be seen by comparing the mode shapes with variations of frequencies as functions of the power-law exponent p. For examples, the frequencies $f_{3,4}$ and f_7 of the parabolic dome of Fig. 15 correspond to bending and axisymmetric mode shape as can be observed from Fig. 10, respectively. However, this behaviour depends on the geometry of the shell and on its boundary conditions.

Finally, in Fig. 16 the influence of the parameter c on the dynamic vibration of parabolic panel (C-F-F-F) is investigated by considering $a=1,b=1$. The parameter c varies from 1 to 11. It can be noted that due to the effect of the parameter c frequencies exhibit a fastly rising behaviour up to a maximum value exceeding the ceramic limit case ($p=0$) by varying the power-law index from $p=0$ to $p\approx 10$. After this maximum, frequencies gradually decrease by increasing the power-law exponent p and tend to the metal limit case ($p=\infty$). The value of the

ACCEPTED MANUSCRIPT

maximum depends on the value of c. By increasing the value of the parameter c ($c>1$) the maximum gradually decreases.

In order to investigate the GDQ procedure convergence, the first ten frequencies of the functionally graded toro-parabolic panel (C-F-C-F) for the $FGM_{1\,(a=1/b=0/c=0/p=5)}$ power-law distribution are examinated by varying the number of grid points. Results are collected in Table 7 when the number of points of the Chebyshev-Gauss-Lobatto grid distribution (26) is increased from $N=M=11$ up to $N=M=31$. It can be seen that the proposed GDQ formulation well captures the dynamic behaviour of the system by using only 21 points in two co-ordinate directions. It can also be seen that for the system under investigation, the formulation is stable while increasing the number of points and that the use of 21 points guarantees convergence of the procedure. Analogous and similar convergence results can be obtained for all the shell structures considered in this work. A wide convergence study of GDQ solutions for shell structures has been shown in the PhD thesis by Tornabene (2007) and in the articles by Tornabene and Viola (2007, 2008).

6. Conclusion Remarks and Summary

The Generalized Differential Quadrature Method has been used to study the free vibration analysis of functionally graded parabolic thick panels and shells of revolution. The First-order Shear Deformation Theory has been adopted. The dynamic equilibrium equations discretized with the present method lead to a standard linear eigenvalue problem. The complete 2D differential system, governing the structural problem, has been solved. The vibration results are obtained without the modal expansion methodology. Thus, complete revolution shells are obtained as special cases of shell panels by satisfying the kinematic and physical compatibility. The GDQ method provides converging results for all the cases as the number of grid points increases. Convergence and stability have been shown for one of the four structures considered.

In this study, ceramic-metal graded shells of revolution with four parameter power-law distributions of the volume fraction of the constituents in the thickness direction have been worked out. Various material profiles through the functionally graded shell thickness have been illustrated by varying the four parameters of power-law distributions. Symmetric and asymmetric volume fraction profiles have been presented. The numerical results have shown the influence of the power-law exponent, of the power-law distribution choice and of the choice of the four parameters on the free vibrations of functionally graded shells considered. The analysis provides information about the dynamic response of parabolic shell structures for different proportions of the ceramic and metal. For curved shells and panels, it has been observed that the influence of the distribution choice is marked and can be considered from the

ACCEPTED MANUSCRIPT

structural design point of view. In general, it can be pointed out that the frequency vibration of functionally graded shells and panels of revolution depends on the type of vibration mode, thickness, power-law distribution, power-law exponent and the curvature of the structure.

Acknowledgments

This research was supported by the Italian Ministry for University and Scientific, Technological Research MIUR (40% and 60%). The research topic is one of the subjects of the Centre of Study and Research for the Identification of Materials and Structures (CIMEST)-"M. Capurso" of the University of Bologna (Italy).

References

Abrate, S., 2006. Free vibration, buckling, and static deflection of functionally graded plates, Compos. Sci. Technol. 66, 2383-2394.

Alfano, G., Auricchio, F., Rosati, L., Sacco, E., 2001. MITC finite elements for laminated composite plates, Int. J. Numer. Meth. Eng. 50, 707-738.

Arciniega, R.A., Reddy, J.N., 2007. Large deformation analysis of functionally graded shells, Int. J. Solids Struct. 44, 2036-2052.

Artioli, E., Gould, P., Viola, E., 2005. A differential quadrature method solution for shear-deformable shells of revolution, Eng. Struct. 27, 1879-1892.

Artioli, E., Viola, E., 2005. Static analysis of shear-deformable shells of revolution via G.D.Q. method, Struct. Eng. Mech. 19, 459-475.

Artioli, E., Viola, E., 2006. Free vibration analysis of spherical caps using a G.D.Q. numerical solution, J. Press Vessel-Tech. ASME 128, 370-378.

Auricchio, F., Sacco, E., 1999. A mixed-enhanced finite-element for the analysis of laminated composite plates, Int. J. Numer. Meth. Eng. 44, 1481-1504.

Auricchio, F., Sacco, E., 2003. Refined first-order shear deformation theory models for composite laminates. J. Appl. Mech. 70, 381-390.

Della Croce, L., Venini, P., 2004. Finite elements for functionally graded Reissner-Mindlin plates, Comput. Methods Appl. Mech. Engrg. 193, 705-725.

Elishakoff, I., Gentilini, C., Viola, E., 2005. Forced vibrations of functionally graded plates in the three-dimensional setting, AIAA J. 43, 2000-2007.

ACCEPTED MANUSCRIPT

Elishakoff, I., Gentilini, C., Viola, E., 2005. Three-dimensional analysis of an all-around clamped plate made of functionally graded materials, Acta Mech. 180, 21-36.

Liew, K.M., He, X.Q., Kitipornchai, S., 2004. Finite element method for the feedback control of FGM shells in the frequency domain via piezoelectric sensors and actuators, Comput. Methods Appl. Mech. Engrg. 193, 257-273.

Marzani, A., Tornabene, F., Viola, E., 2008. Nonconservative Stability Problems via Generalized Differential Quadrature Method, J. Sound Vib. 315, 176-196.

Ng, T.Y., Lam, K.Y., Liew, K.M., 2000. Effect of FGM materials on the parametric resonance of plate structures, Comput. Methods Appl. Mech. Engrg. 190, 953-962.

Nie, G.J., Zhong, Z., 2007. Semi-analytical solution for three dimensional vibration of functionally graded circular plates, Comput. Methods Appl. Mech. Engrg. 196, 4901-4910.

Patel, B.P., Gupta, S.S., Loknath, M.S., Kadu, C.P., 2005. Free vibration analysis of functionally graded elliptical cylindrical shells using higher-order theory, Compos. Struct. 69, 259-270.

Pelletier, J.L., Vel, S.S., 2006. An exact solution for the steady-state thermoelastic response of functionally graded orthotropic cylindrical shells, Int. J. Solids Struct. 43, 1131-1158.

Reddy, J.N., 2003. Mechanics of Laminated Composites Plates and Shells, CRC Press, New York.

Roque, C.M.C., Ferreira, A.J.M., Jorge, R.M.N., 2007. A radial basis function for the free vibration analysis of functionally graded plates using refined theory, J. Sound Vib. 300, 1048-1070.

Shu, C., 2000. Differential Quadrature and Its Application in Engineering, Springer, Berlin.

Toorani, M.H., Lakis, A.A., 2000. General equations of anisotropic plates and shells including transverse shear deformations, rotary inertia and initial curvature effects, J. Sound Vib. 237, 561-615.

Tornabene, F., 2007. Modellazione e Soluzione di Strutture a Guscio in Materiale Anisotropo, PhD Thesis, University of Bologna – DISTART Department.

Tornabene, F., Viola, E., 2007. Vibration analysis of spherical structural elements using the GDQ method, Comput. Math. Appl. 53, 1538-1560.

Tornabene, F., Viola, E., 2008. 2-D Solution for free vibrations of parabolic shells using generalized differential quadrature method, Eur. J. Mech. A/Solids, Available online 4 march 2008.

Viola, E., Artioli, E., 2004. The G.D.Q. method for the harmonic dynamic analysis of rotational shell structural elements, Struct. Eng. Mech. 17, 789-817.

Viola, E., Dilena, M., Tornabene, F., 2007. Analytical and numerical results for vibration analysis of multi-stepped and multi-damaged circular arches, J. Sound Vib. 299, 143-163.

ACCEPTED MANUSCRIPT

Viola, E., Tornabene, F., 2005. Vibration analysis of damaged circular arches with varying cross-section, Struct. Integr. Durab. (SID-SDHM) 1, 155-169.

Viola, E., Tornabene, F., 2006. Vibration analysis of conical shell structures using GDQ method, Far East J. Appl. Math. 25, 23-39.

Yang, J., Kitipornchai, S., Liew, K.M., 2003. Large amplitude vibration of thermo-electro-mechanically stressed FGM laminated plates, Comput. Methods Appl. Mech. Engrg. 192, 3861-3885.

Yang, J., Shen, H.S., 2007. Free vibration and parametric resonance of shear deformable functionally graded cylindrical panels, J. Sound Vib. 261, 871-893.

Wu, C.P., Tsai, Y.H., 2004. Asymptotic DQ Solutions of Functionally Graded Annular Spherical Shells, Eur. J. Mech A-Solids 23, 283-299.

Zenkour, A.M., 2006. Generalized shear deformation theory for bending analysis of functionally graded plates, Appl. Math. Model. 30, 67-84.

Appendix

The following are the equilibrium operators in equations (10):

$$L_{11}=\frac{A_{11}}{R_\varphi^2}\frac{\partial^2}{\partial\varphi^2}+A_{11}\left(\frac{\cos\varphi}{R_\varphi R_0}-\frac{1}{R_\varphi^3}\frac{dR_\varphi}{d\varphi}\right)\frac{\partial}{\partial\varphi}+A_{66}\frac{\partial^2}{\partial s^2}-\frac{A_{12}\sin\varphi}{R_\varphi R_0}-\frac{A_{11}\cos^2\varphi}{R_0^2}-\kappa\frac{A_{66}}{R_\varphi^2}$$

$$L_{12}=-\left(\frac{A_{11}\cos\varphi}{R_0}+\frac{A_{66}\cos\varphi}{R_0}\right)\frac{\partial}{\partial s}+\left(\frac{A_{12}}{R_\varphi}+\frac{A_{66}}{R_\varphi}\right)\frac{\partial^2}{\partial\varphi\partial s}$$

$$L_{13}=\left(\frac{A_{11}}{R_\varphi^2}+\frac{A_{12}\sin\varphi}{R_\varphi R_0}+\kappa\frac{A_{66}}{R_\varphi^2}\right)\frac{\partial}{\partial\varphi}+A_{11}\left(\frac{\cos\varphi}{R_\varphi R_0}-\frac{1}{R_\varphi^3}\frac{dR_\varphi}{d\varphi}\right)-\frac{A_{11}\sin\varphi\cos\varphi}{R_0^2}$$

$$L_{14}=L_{41}=\frac{B_{11}}{R_\varphi^2}\frac{\partial^2}{\partial\varphi^2}+B_{11}\left(\frac{\cos\varphi}{R_\varphi R_0}-\frac{1}{R_\varphi^3}\frac{dR_\varphi}{d\varphi}\right)\frac{\partial}{\partial\varphi}+B_{66}\frac{\partial^2}{\partial s^2}-\frac{B_{12}\sin\varphi}{R_\varphi R_0}-\frac{B_{11}\cos^2\varphi}{R_0^2}+\kappa\frac{A_{66}}{R_\varphi}$$

$$L_{15}=L_{42}=-\left(\frac{B_{11}\cos\varphi}{R_0}+\frac{B_{66}\cos\varphi}{R_0}\right)\frac{\partial}{\partial s}+\left(\frac{B_{12}}{R_\varphi}+\frac{B_{66}}{R_\varphi}\right)\frac{\partial^2}{\partial\varphi\partial s}$$

$$L_{21}=\left(\frac{A_{11}\cos\varphi}{R_0}+\frac{A_{66}\cos\varphi}{R_0}\right)\frac{\partial}{\partial s}+\left(\frac{A_{12}}{R_\varphi}+\frac{A_{66}}{R_\varphi}\right)\frac{\partial^2}{\partial\varphi\partial s}$$

$$L_{22}=\frac{A_{66}}{R_\varphi^2}\frac{\partial^2}{\partial\varphi^2}+A_{66}\left(\frac{\cos\varphi}{R_\varphi R_0}-\frac{1}{R_\varphi^3}\frac{dR_\varphi}{d\varphi}\right)\frac{\partial}{\partial\varphi}+A_{11}\frac{\partial^2}{\partial s^2}-A_{66}\left(\frac{\cos^2\varphi}{R_0^2}-\frac{\sin\varphi}{R_\varphi R_0}\right)-\kappa\frac{A_{66}\sin^2\varphi}{R_0^2}$$

$$L_{23}=-L_{32}=\left(\frac{A_{12}}{R_\varphi}+\frac{A_{11}\sin\varphi}{R_0}+\kappa\frac{A_{66}\sin\varphi}{R_0}\right)\frac{\partial}{\partial s}$$

ACCEPTED MANUSCRIPT

$$L_{24}=L_{51}=\left(\frac{B_{11}\cos\varphi}{R_0}+\frac{B_{66}\cos\varphi}{R_0}\right)\frac{\partial}{\partial s}+\left(\frac{B_{12}}{R_\varphi}+\frac{B_{66}}{R_\varphi}\right)\frac{\partial^2}{\partial\varphi\partial s}$$

$$L_{25}=L_{52}=\frac{B_{66}}{R_\varphi^2}\frac{\partial^2}{\partial\varphi^2}+B_{66}\left(\frac{\cos\varphi}{R_\varphi R_0}-\frac{1}{R_\varphi^3}\frac{dR_\varphi}{d\varphi}\right)\frac{\partial}{\partial\varphi}+B_{11}\frac{\partial^2}{\partial s^2}-B_{66}\left(\frac{\cos^2\varphi}{R_0^2}-\frac{\sin\varphi}{R_\varphi R_0}\right)+\kappa\frac{A_{66}\sin\varphi}{R_0}$$

$$L_{31}=-\left(\frac{A_{11}}{R_\varphi^2}+\frac{A_{12}\sin\varphi}{R_\varphi R_0}+\kappa\frac{A_{66}}{R_\varphi^2}\right)\frac{\partial}{\partial\varphi}-\frac{A_{12}\cos\varphi}{R_\varphi R_0}-\frac{A_{11}\sin\varphi\cos\varphi}{R_0^2}-\kappa A_{66}\left(\frac{\cos\varphi}{R_\varphi R_0}-\frac{1}{R_\varphi^3}\frac{dR_\varphi}{d\varphi}\right)$$

$$L_{33}=\kappa\frac{A_{66}}{R_\varphi^2}\frac{\partial^2}{\partial\varphi^2}+\kappa A_{66}\left(\frac{\cos\varphi}{R_\varphi R_0}-\frac{1}{R_\varphi^3}\frac{dR_\varphi}{d\varphi}\right)\frac{\partial}{\partial\varphi}+\kappa A_{66}\frac{\partial^2}{\partial s^2}-\frac{A_{11}}{R_\varphi^2}-\frac{2A_{12}\sin\varphi}{R_\varphi R_0}-\frac{A_{11}\sin^2\varphi}{R_0^2}$$

$$L_{34}=\left(-\frac{B_{11}}{R_\varphi^2}-\frac{B_{12}\sin\varphi}{R_0R_\varphi}+\kappa\frac{A_{66}}{R_\varphi}\right)\frac{\partial}{\partial\varphi}-\frac{B_{12}\cos\varphi}{R_\varphi R_0}-\frac{B_{11}\sin\varphi\cos\varphi}{R_0^2}+\kappa\frac{A_{66}\cos\varphi}{R_0}$$

$$L_{35}=-L_{53}=\left(-\frac{B_{12}}{R_\varphi}-\frac{B_{11}\sin\varphi}{R_0}+\kappa A_{66}\right)\frac{\partial}{\partial s}$$

$$L_{43}=\left(\frac{B_{11}}{R_\varphi^2}+\frac{B_{12}\sin\varphi}{R_\varphi R_0}-\kappa\frac{A_{66}}{R_\varphi}\right)\frac{\partial}{\partial\varphi}+B_{11}\left(\frac{\cos\varphi}{R_\varphi R_0}-\frac{1}{R_\varphi^3}\frac{dR_\varphi}{d\varphi}\right)-\frac{B_{11}\sin\varphi\cos\varphi}{R_0^2}$$

$$L_{44}=\frac{D_{11}}{R_\varphi^2}\frac{\partial^2}{\partial\varphi^2}+D_{11}\left(\frac{\cos\varphi}{R_\varphi R_0}-\frac{1}{R_\varphi^3}\frac{dR_\varphi}{d\varphi}\right)\frac{\partial}{\partial\varphi}+D_{66}\frac{\partial^2}{\partial s^2}-\frac{D_{12}\sin\varphi}{R_\varphi R_0}-\frac{D_{11}\cos^2\varphi}{R_0^2}-\kappa A_{66}$$

$$L_{45}=-\left(\frac{D_{11}\cos\varphi}{R_0}+\frac{D_{66}\cos\varphi}{R_0}\right)\frac{\partial}{\partial s}+\left(\frac{D_{12}}{R_\varphi}+\frac{D_{66}}{R_\varphi}\right)\frac{\partial^2}{\partial\varphi\partial s}$$

$$L_{54}=\left(\frac{D_{11}\cos\varphi}{R_0}+\frac{D_{66}\cos\varphi}{R_0}\right)\frac{\partial}{\partial s}+\left(\frac{D_{12}}{R_\varphi}+\frac{D_{66}}{R_\varphi}\right)\frac{\partial^2}{\partial\varphi\partial s}$$

$$L_{55}=\frac{D_{66}}{R_\varphi^2}\frac{\partial^2}{\partial\varphi^2}+D_{66}\left(\frac{\cos\varphi}{R_\varphi R_0}-\frac{1}{R_\varphi^3}\frac{dR_\varphi}{d\varphi}\right)\frac{\partial}{\partial\varphi}+D_{11}\frac{\partial^2}{\partial s^2}-D_{66}\left(\frac{\cos^2\varphi}{R_0^2}-\frac{\sin\varphi}{R_\varphi R_0}\right)-\kappa A_{66}$$

ACCEPTED MANUSCRIPT

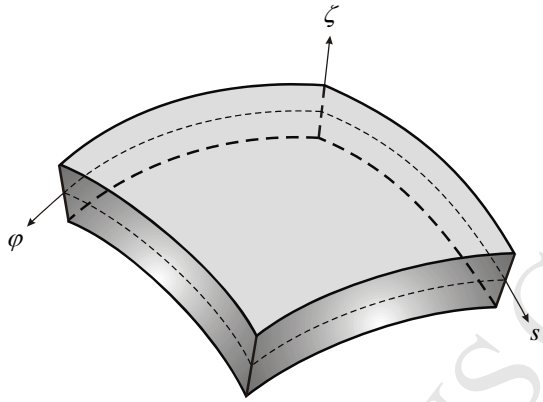

Figure 1. Co-ordinate system of doubly curved shell.

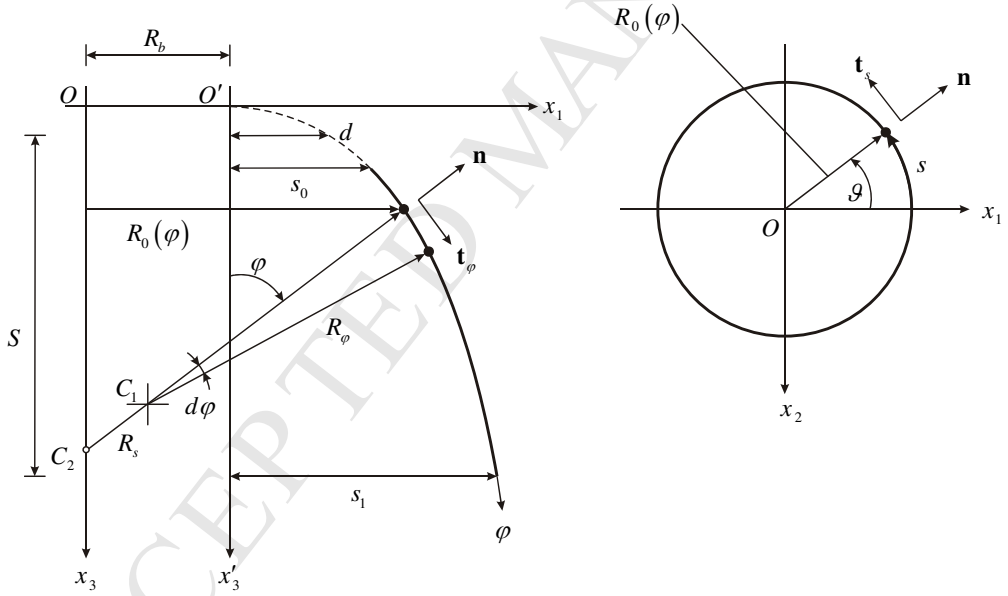

Figure 2. Shell geometry.

ACCEPTED MANUSCRIPT

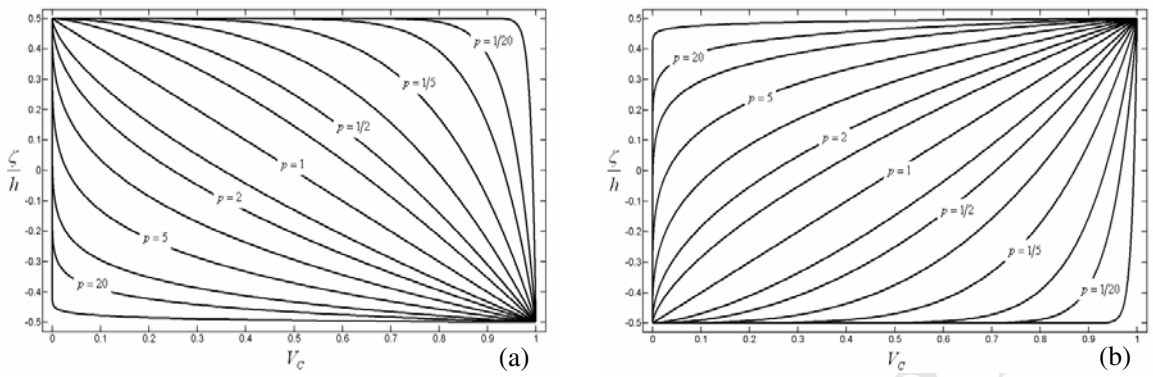

Figure 3. Variations of the ceramic volume fraction V_C through the thickness for different values of the power-law index p: (a) $FGM_{1(a=1/b=0/c/p)}$, (b) $FGM_{2(a=1/b=0/c/p)}$.

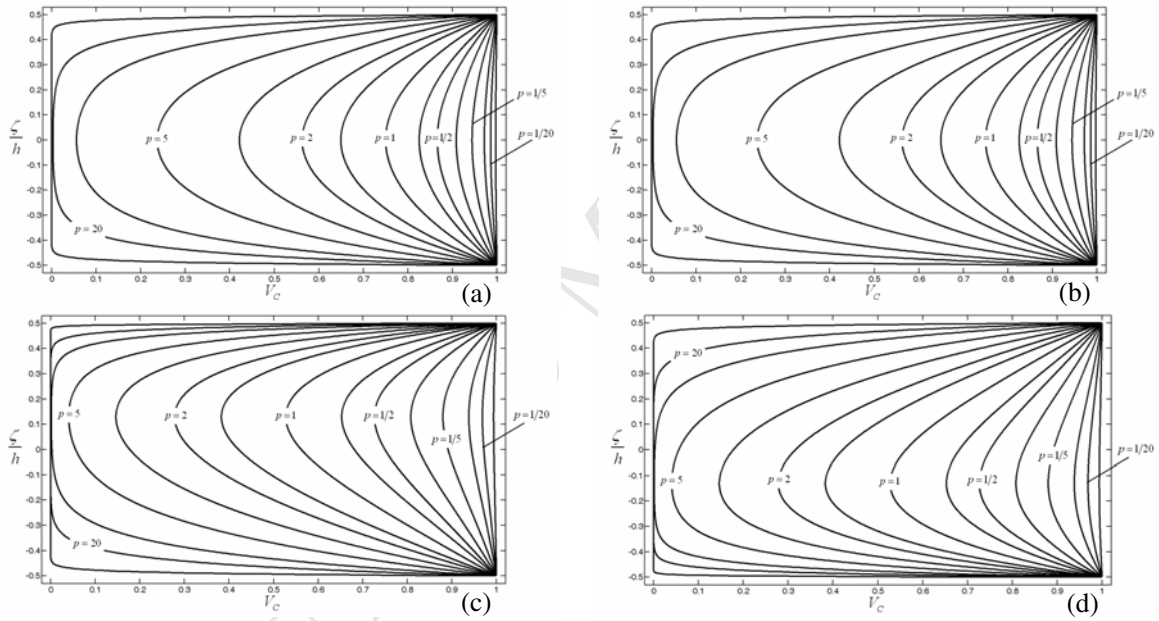

Figure 4. Variations of the ceramic volume fraction V_C through the thickness for different values of the power-law index p: (a) $FGM_{1(a=1/b=1/c=2/p)}$, (b) $FGM_{2(a=1/b=1/c=2/p)}$, (c) $FGM_{1(a=1/b=1/c=4/p)}$, (d) $FGM_{2(a=1/b=1/c=4/p)}$.

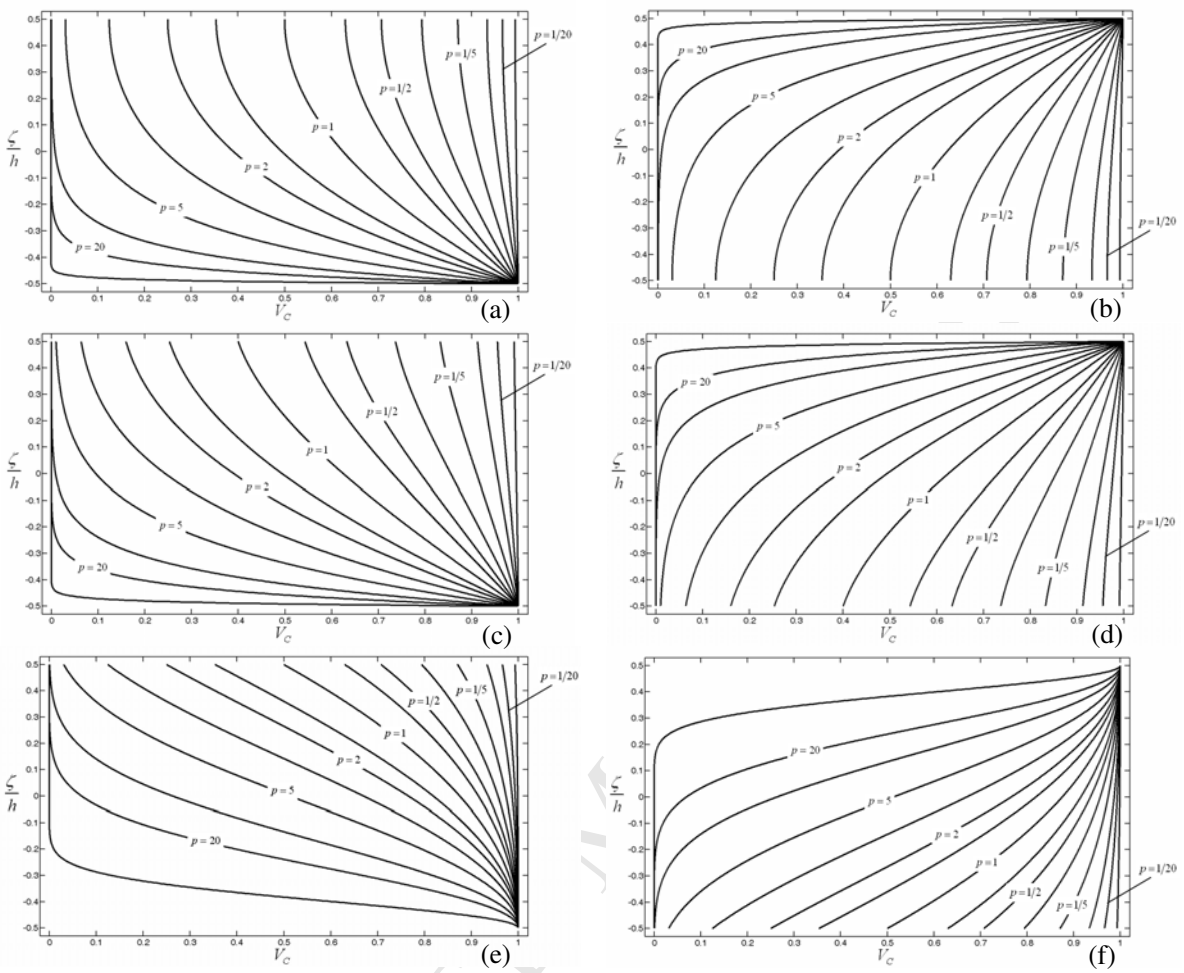

Figure 5. Variations of the ceramic volume fraction V_C through the thickness for different values of the three parameters a,b,c and the power-law index p: (a) $FGM_{1\,(a=1/b=0.5/c=2/p)}$, (b) $FGM_{2\,(a=1/b=0.5/c=2/p)}$, (c) $FGM_{1\,(a=0.8/b=0.2/c=3/p)}$, (d) $FGM_{2\,(a=0.8/b=0.2/c=3/p)}$, (e) $FGM_{1\,(a=0/b=0.5/c=2/p)}$, (f) $FGM_{2\,(a=0/b=0.5/c=2/p)}$.

ACCEPTED

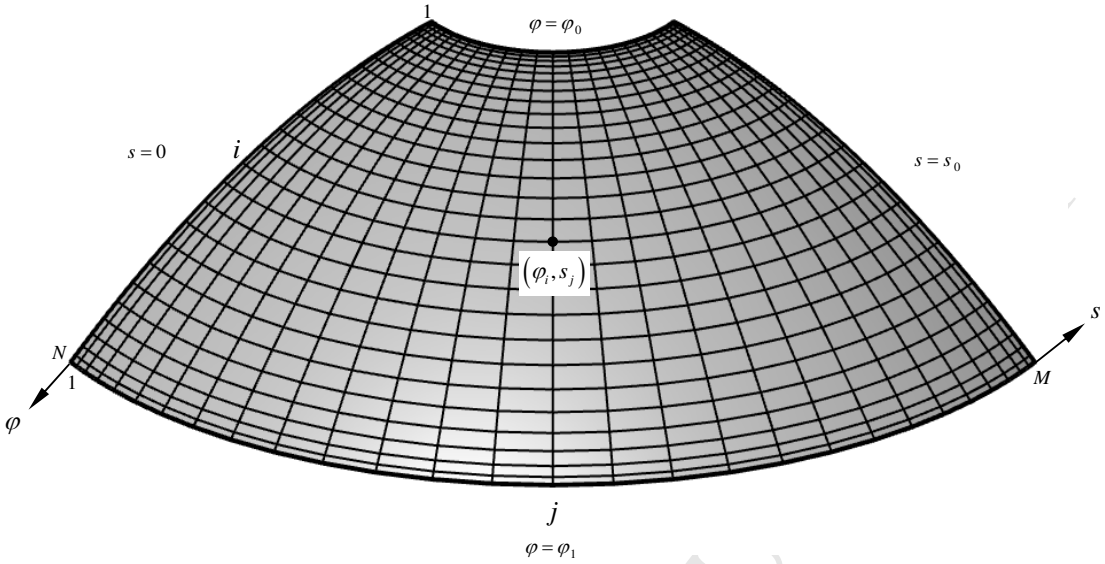

Figure 6. C-G-L grid distribution on a parabolic panel.

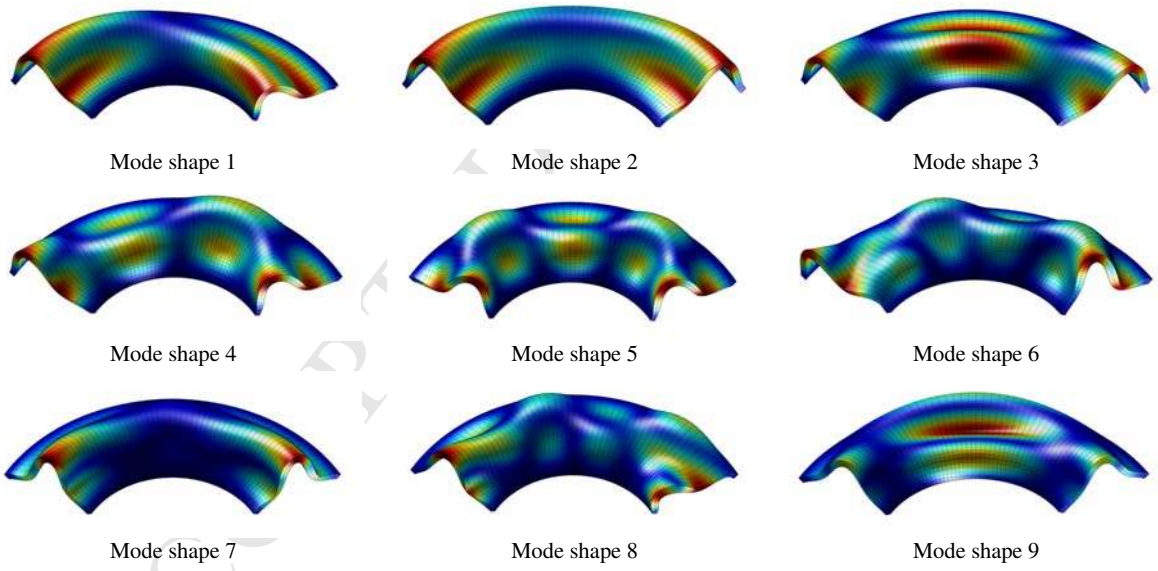

Figure 7. Mode shapes for the $FGM_{1\,(a=1/b=0.5/c=2/p=1)}$ toro-parabolic panel C-F-C-F.

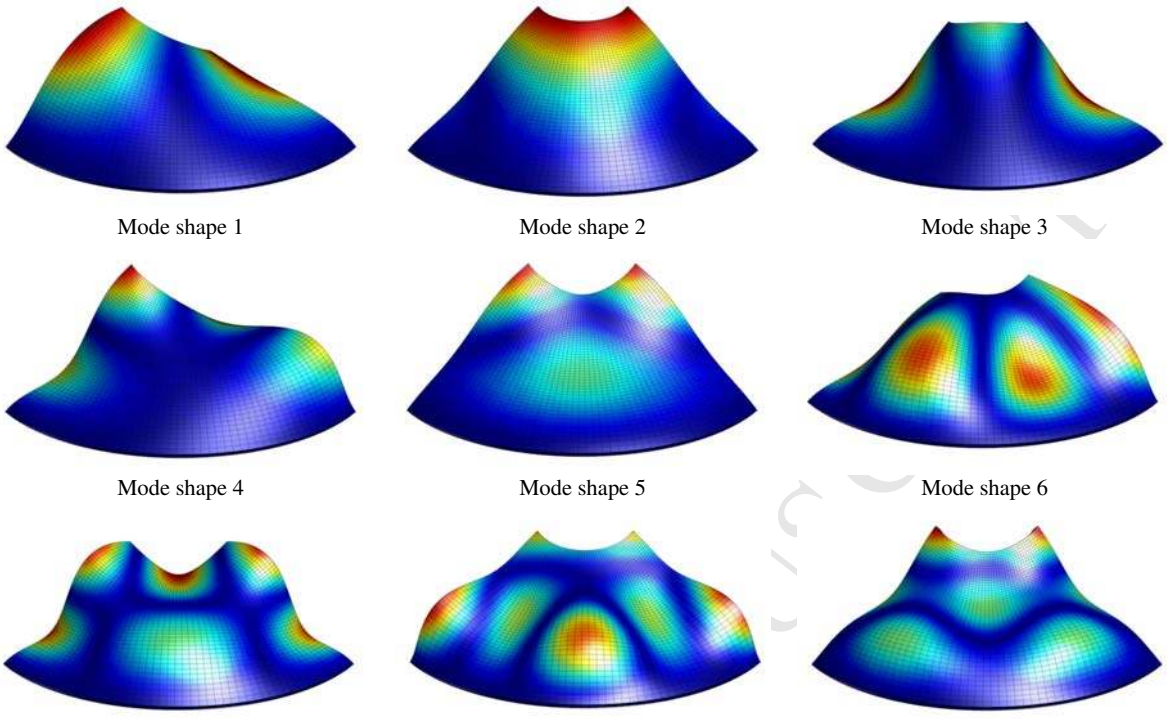

Mode shape 1 | Mode shape 2 | Mode shape 3

Mode shape 4 | Mode shape 5 | Mode shape 6

Mode shape 7 | Mode shape 8 | Mode shape 9

Figure 8. Mode shapes for the $FGM_{1\,(a=1/b=1/c=3/\,p=1)}$ parabolic panel C-F-F-F.

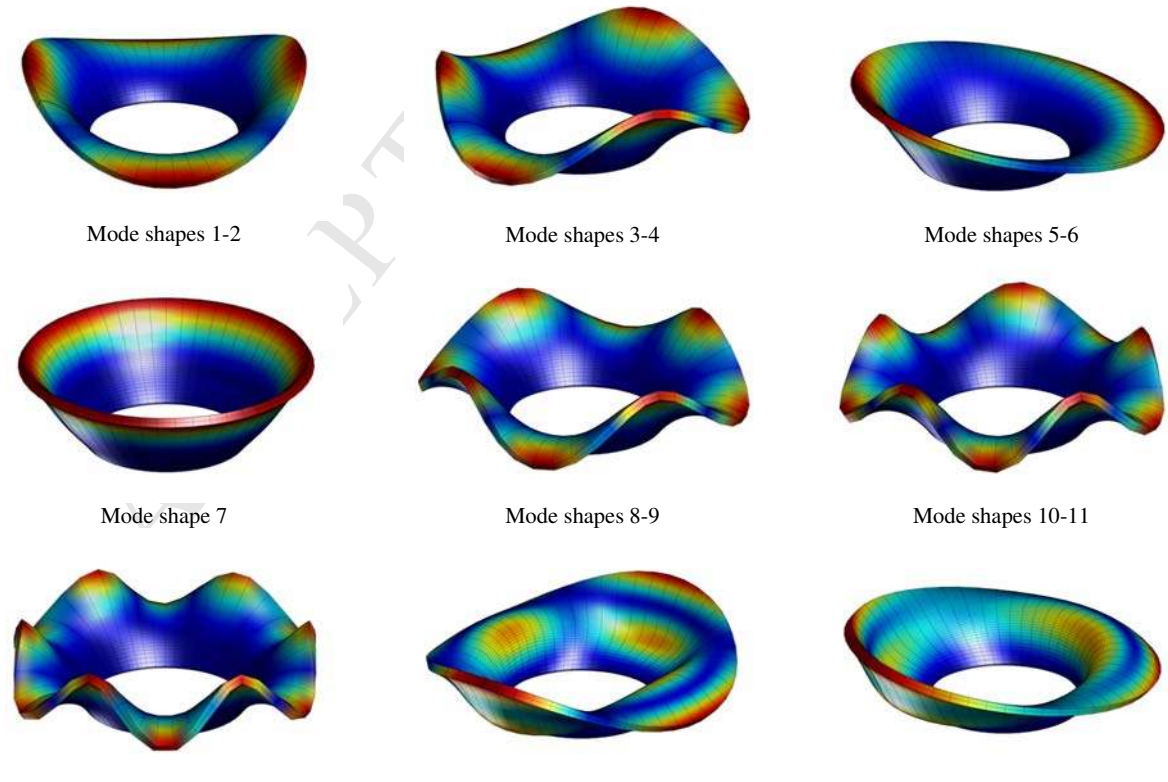

Mode shapes 1-2 | Mode shapes 3-4 | Mode shapes 5-6

Mode shape 7 | Mode shapes 8-9 | Mode shapes 10-11

Mode shapes 12-13 | Mode shapes 14-15 | Mode shapes 16-17

Figure 9. Mode shapes for the $FGM_{1\,(a=0/b=-0.5/c=2/\,p=1)}$ parabolic toroid F-C.

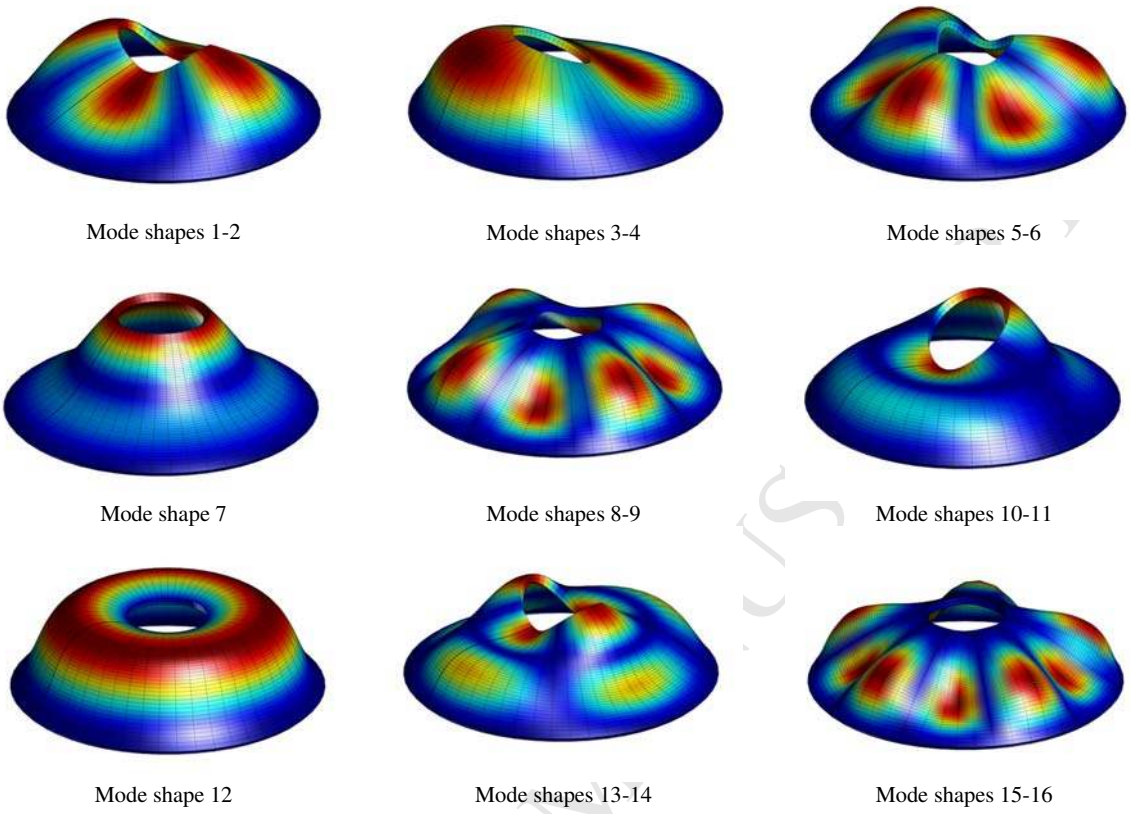

Figure 10. Mode shapes for the $FGM_{1(a=0.8/b=0.2/c=3/p=1)}$ parabolic dome C-F.

ACCEPTED MANUSCRIPT

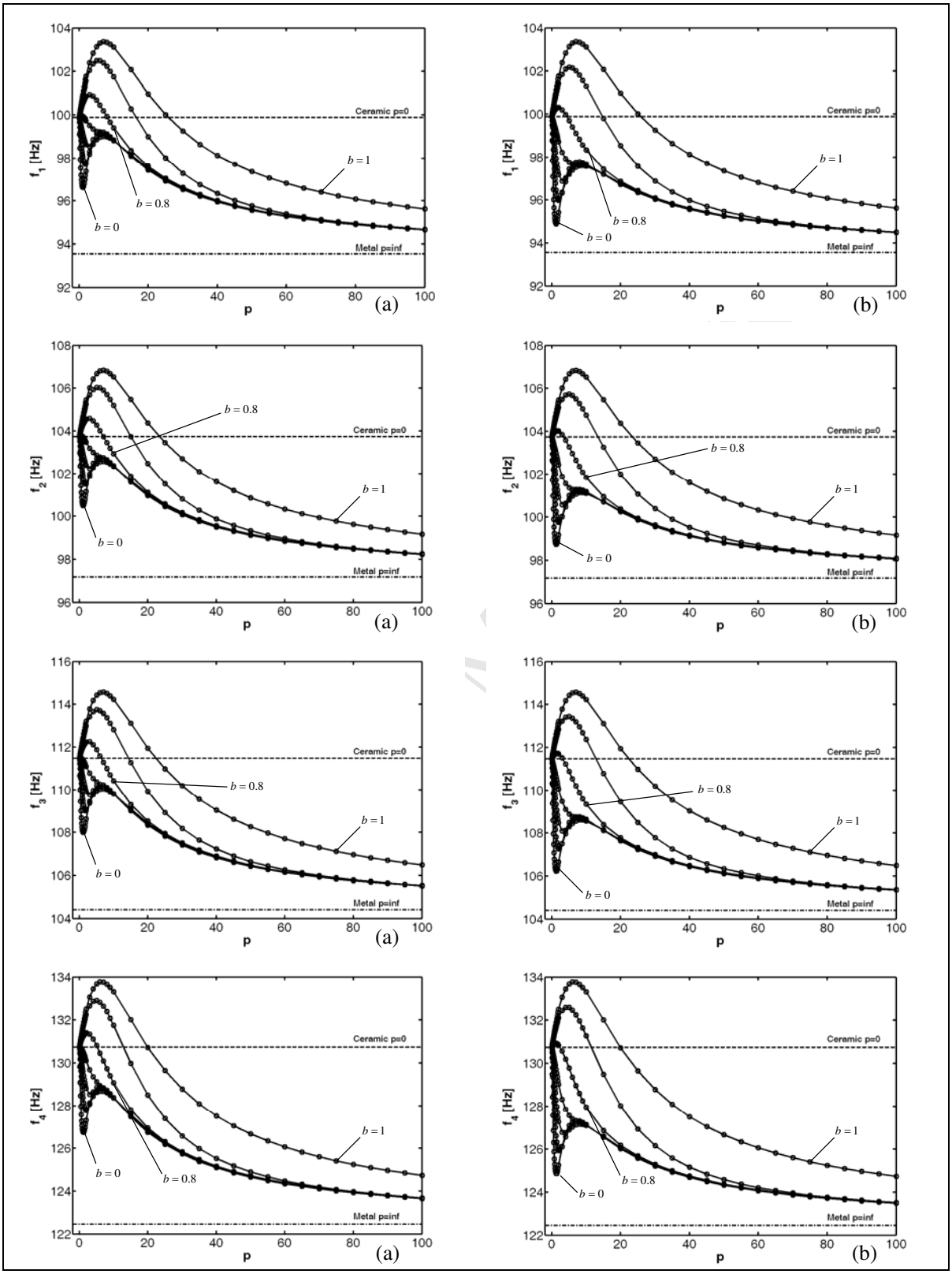

Figure 11. The first four frequencies of functionally graded toro-parabolic panel (C-F-C-F) versus the power-law exponent p for various values of the parameter b : (a) $FGM_{1\,(a=1/0\le b\le 1/c=2/p)}$, (b) $FGM_{2\,(a=1/0\le b\le 1/c=2/p)}$.

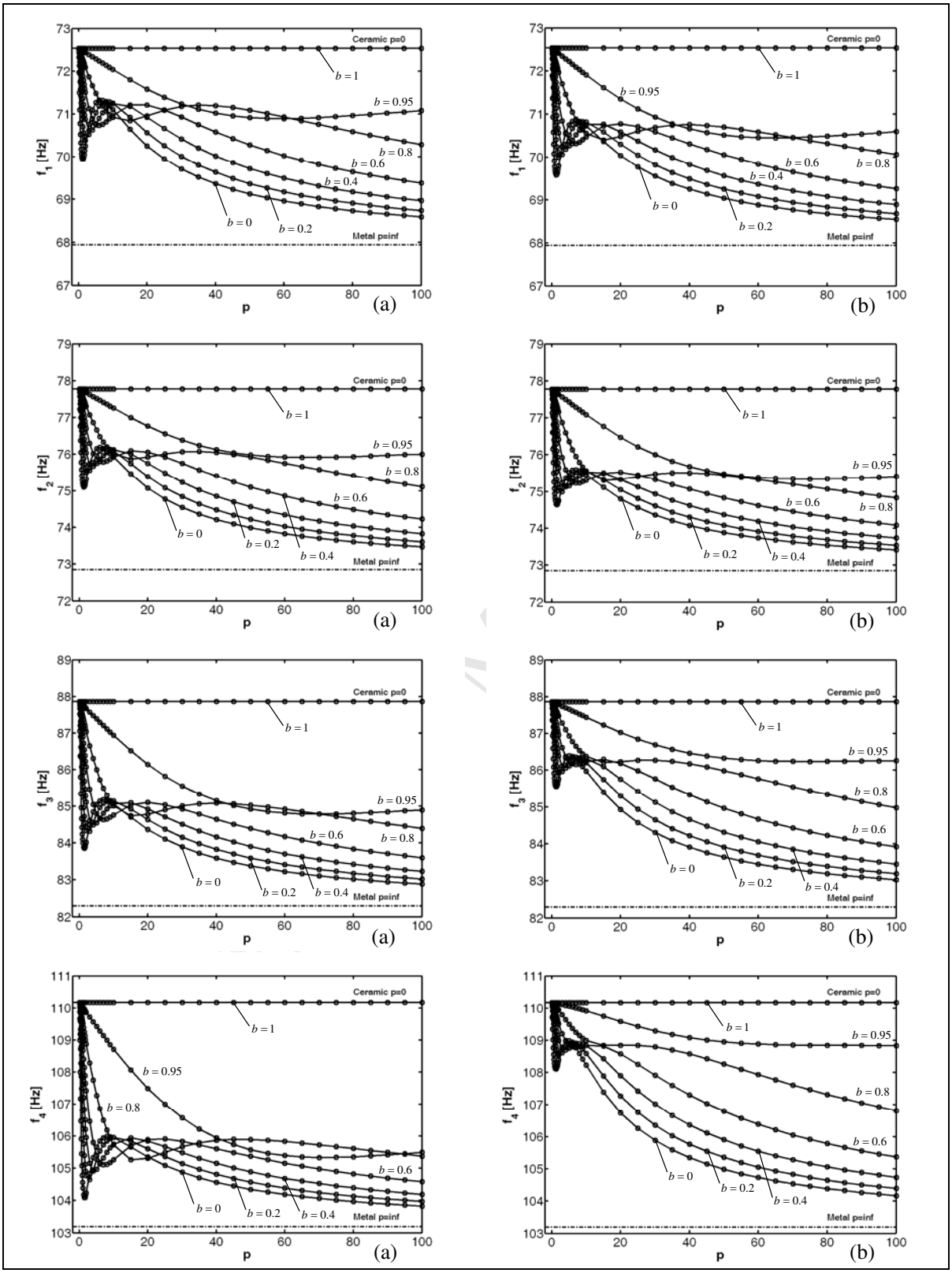

Figure 12. The first four frequencies of functionally graded toro-parabolic panel (S-F-S-F) versus the power-law exponent p for various values of the parameter b : (a) $FGM_{1\,(a=1/0\le b\le 1/c=1/p)}$, (b) $FGM_{2\,(a=1/0\le b\le 1/c=1/p)}$.

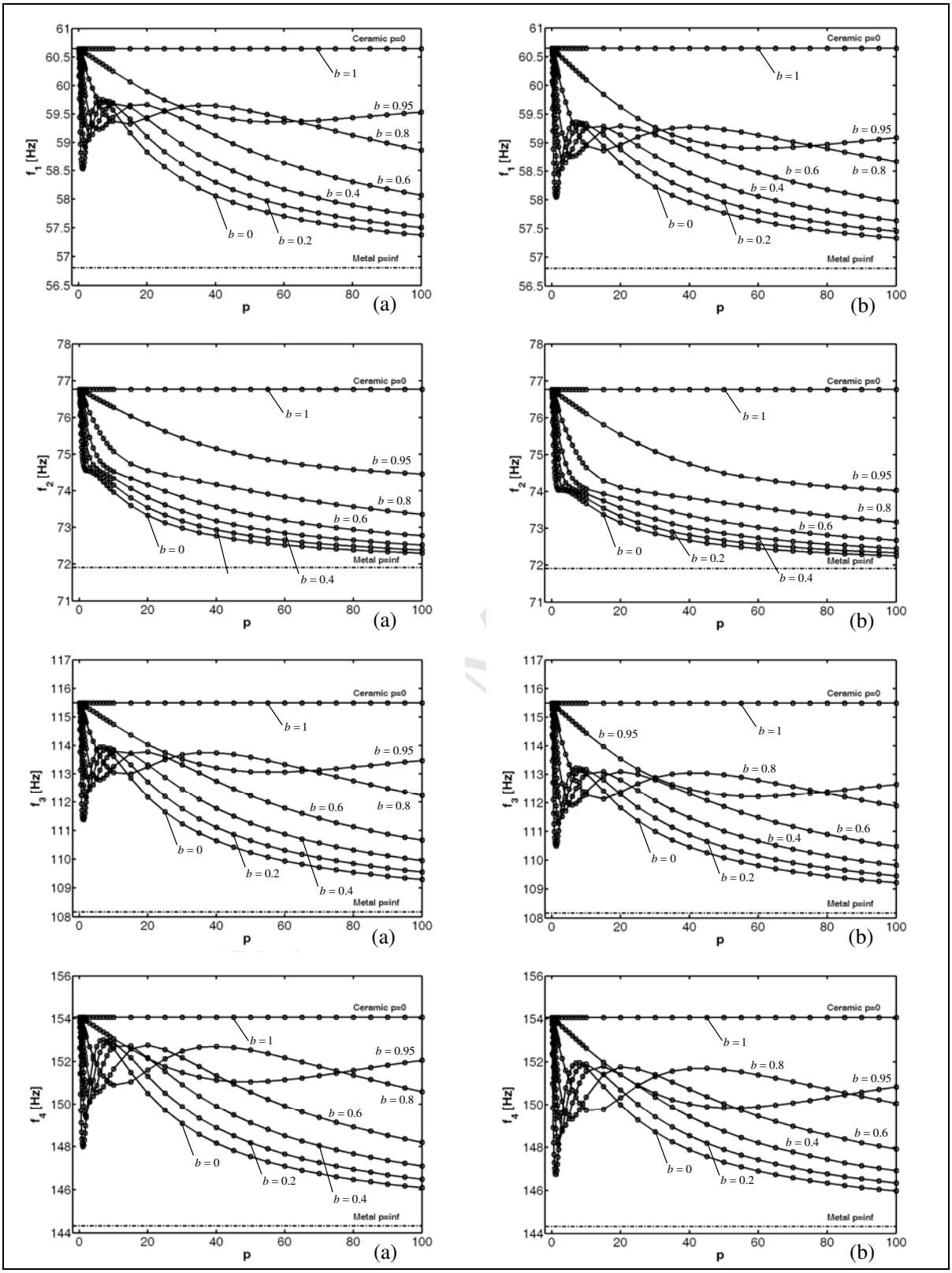

Figure 13. The first four frequencies of functionally graded parabolic panel (C-F-F-F) versus the power-law exponent p for various values of the parameter b : (a) $FGM_{1\,(a=1/0\le b\le 1/c=1/p)}$, (b) $FGM_{2\,(a=1/0\le b\le 1/c=1/p)}$.

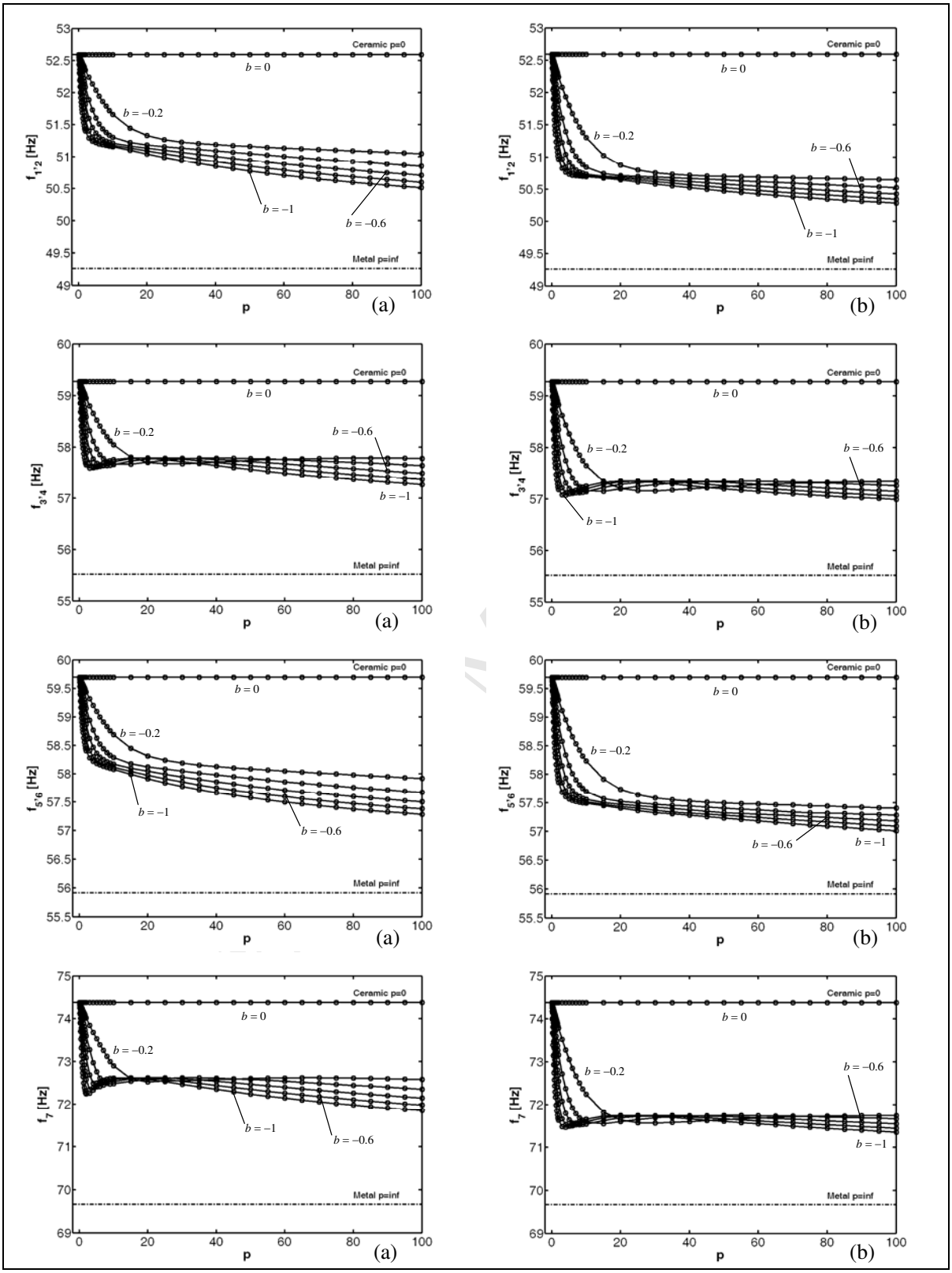

Figure 14. The first four frequencies of functionally graded parabolic toroid (F-C) versus the power-law exponent p for various values of the parameter b : (a) $FGM_{1\,(a=0/-1\le b\le 0/c=2/p)}$, (b) $FGM_{2\,(a=0/-1\le b\le 0/c=2/p)}$.

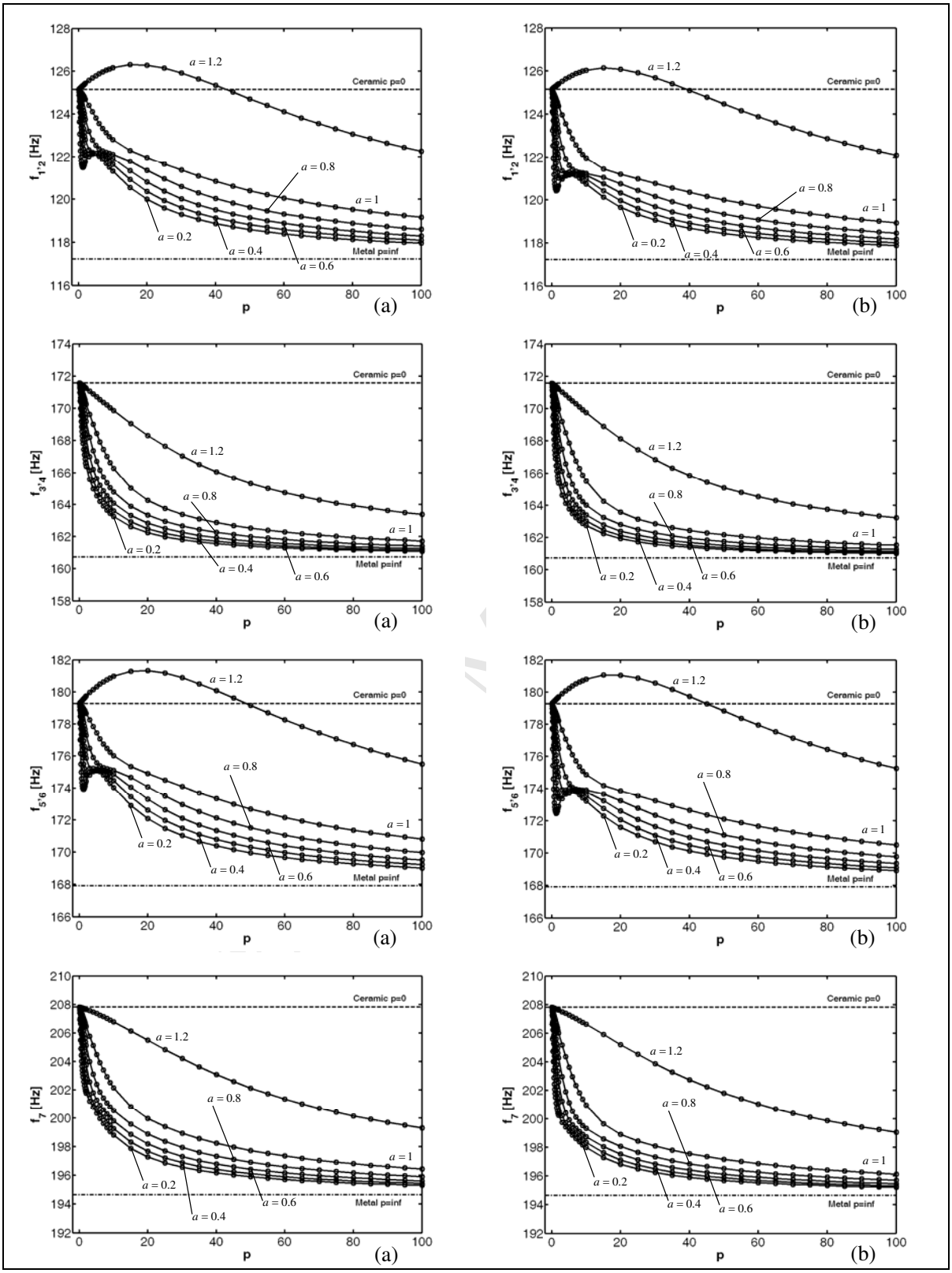

Figure 15. The first four frequencies of functionally graded parabolic dome (C-F) versus the power-law exponent p for various values of the parameter a : (a) $FGM_{1\,(0.2\le a\le 1.2/b=0.2/c=3/p)}$, (b) $FGM_{2\,(0.2\le a\le 1.2/b=0.2/c=3/p)}$.

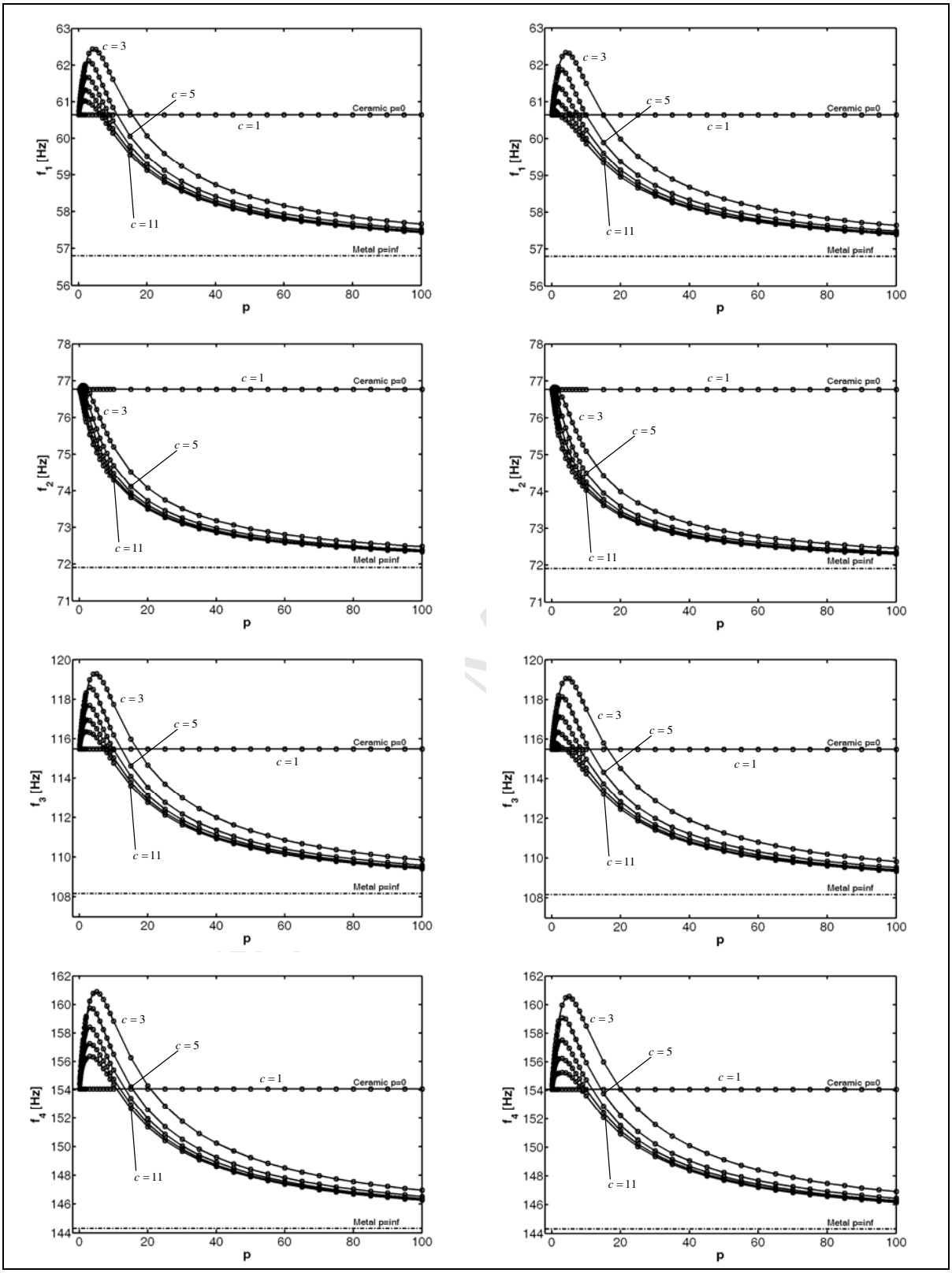

Figure 16. The first four frequencies of functionally graded parabolic panel (C-F-F-F) versus the power-law exponent p for various values of the parameter c: (a) $FGM_{1\,(a=1/b=1/1\le c\le 11/\,p)}$, (b) $FGM_{2\,(a=1/b=1/1\le c\le 11/\,p)}$.

Table 1. The first ten frequencies for the functionally graded toro-parabolic panel (C-F-C-F) as a function of the power-law exponent p, for $a=1, b=0.5, c=2$.

$FGM_{1\,(a=1/b=0.5/c=2/p)}$ power-law distribution								
Frequencies [Hz]	$p=0$	$p=0.6$	$p=1$	$p=5$	$p=20$	$p=50$	$p=100$	$p=\infty$
f_1	99.88	99.73	99.57	98.95	97.51	95.59	94.66	93.56
f_2	103.74	103.55	103.36	102.57	101.03	99.15	98.24	97.17
f_3	111.46	111.23	111.01	110.06	108.42	106.46	105.52	104.41
f_4	130.73	130.40	130.11	128.77	126.84	124.69	123.67	122.45
f_5	158.23	157.76	157.38	155.49	153.14	150.72	149.57	148.21
f_6	184.79	184.26	183.82	181.53	178.67	175.96	174.66	173.09
f_7	191.80	191.39	191.02	189.01	185.90	182.89	181.43	179.65
f_8	193.54	192.97	192.51	189.94	186.85	184.15	182.86	181.29
f_9	202.18	201.81	201.45	199.68	196.50	193.07	191.40	189.38
f_{10}	208.93	208.32	207.83	205.00	201.62	198.76	197.38	195.70
$FGM_{2\,(a=1/b=0.5/c=2/p)}$ power-law distribution								
Frequencies [Hz]	$p=0$	$p=0.6$	$p=1$	$p=5$	$p=20$	$p=50$	$p=100$	$p=\infty$
f_1	99.88	99.24	98.81	97.36	96.78	95.27	94.50	93.56
f_2	103.74	103.05	102.59	100.96	100.29	98.82	98.08	97.17
f_3	111.46	110.73	110.24	108.46	107.69	106.14	105.36	104.41
f_4	130.73	129.88	129.30	127.10	126.07	124.36	123.50	122.45
f_5	158.23	157.19	156.50	153.69	152.32	150.36	149.39	148.21
f_6	184.79	183.53	182.70	179.27	177.65	175.51	174.42	173.09
f_7	191.80	190.43	189.54	185.98	184.51	182.28	181.11	179.65
f_8	193.54	192.18	191.29	187.51	185.74	183.66	182.60	181.29
f_9	202.18	200.79	199.86	196.38	194.98	192.39	191.05	189.38
f_{10}	208.93	207.45	206.48	202.32	200.40	198.22	197.10	195.70

ACCEPTED MANUSCRIPT

Table 2. The first ten frequencies for the functionally graded toro-parabolic panel (S-F-S-F) as a function of the power-law exponent p, for $a=1, b=0.5, c=1$.

$FGM_{1\,(a=1/b=0.5/c=1/p)}$ power-law distribution								
Frequencies [Hz]	$p=0$	$p=0.6$	$p=1$	$p=5$	$p=20$	$p=50$	$p=100$	$p=\infty$
f_1	72.54	72.08	71.79	70.69	71.10	69.96	69.14	67.94
f_2	77.77	77.31	77.01	75.74	75.93	74.80	74.00	72.85
f_3	87.86	87.06	86.57	84.57	85.04	84.12	83.38	82.30
f_4	110.17	108.93	108.18	105.03	105.92	105.11	104.36	103.19
f_5	139.09	137.67	136.81	133.14	134.08	132.92	131.89	130.28
f_6	152.89	152.32	151.89	150.65	152.21	149.02	146.65	143.21
f_7	155.81	155.13	154.65	153.20	154.73	151.56	149.25	145.94
f_8	164.79	163.98	163.42	161.66	163.45	160.26	157.86	154.36
f_9	171.59	169.95	168.95	164.70	165.55	163.98	162.69	160.73
f_{10}	176.50	175.32	174.56	172.14	174.42	171.28	168.86	165.33
$FGM_{2\,(a=1/b=0.5/c=1/p)}$ power-law distribution								
Frequencies [Hz]	$p=0$	$p=0.6$	$p=1$	$p=5$	$p=20$	$p=50$	$p=100$	$p=\infty$
f_1	72.54	71.97	71.62	70.25	70.71	69.79	69.05	67.94
f_2	77.77	77.17	76.80	75.19	75.45	74.58	73.89	72.85
f_3	87.86	87.47	87.22	86.12	85.99	84.60	83.65	82.30
f_4	110.17	109.92	109.72	108.75	108.26	106.29	105.00	103.19
f_5	139.09	138.58	138.21	136.51	136.39	134.08	132.51	130.28
f_6	152.89	151.09	149.99	145.97	148.89	147.38	145.78	143.21
f_7	155.81	154.15	153.15	149.47	151.78	150.13	148.52	145.94
f_8	164.79	163.09	162.04	158.24	160.94	159.03	157.21	154.36
f_9	171.59	170.91	170.42	168.16	167.92	165.18	163.34	160.73
f_{10}	176.50	175.04	174.14	171.12	173.11	170.68	168.58	165.33

ACCEPTED MANUSCRIPT

Table 3. The first ten frequencies for the functionally graded parabolic panel (C-F-F-F) as a function of the power-law exponent p, for $a=1, b=0.5, c=1$.

$FGM_{1\,(a=1/b=0.5/c=1/p)}$ power-law distribution								
Frequencies [Hz]	$p=0$	$p=0.6$	$p=1$	$p=5$	$p=20$	$p=50$	$p=100$	$p=\infty$
f_1	60.64	60.27	60.04	59.19	59.56	58.59	57.86	56.80
f_2	76.77	76.36	76.11	74.75	73.98	73.14	72.63	71.90
f_3	115.49	114.77	114.31	112.72	113.60	111.69	110.25	108.17
f_4	154.07	153.07	152.43	150.55	152.57	149.76	147.57	144.32
f_5	170.55	169.65	169.08	166.19	164.95	162.88	161.57	159.75
f_6	215.38	214.11	213.31	210.11	210.62	207.39	205.07	201.74
f_7	244.57	243.02	242.03	238.87	241.38	237.12	233.87	229.08
f_8	283.57	281.78	280.64	276.89	279.48	274.67	271.00	265.61
f_9	289.98	288.19	287.04	283.04	285.08	280.34	276.80	271.62
f_{10}	302.10	300.14	298.89	295.03	298.26	293.07	289.04	282.97
$FGM_{2\,(a=1/b=0.5/c=1/p)}$ power-law distribution								
Frequencies [Hz]	$p=0$	$p=0.6$	$p=1$	$p=5$	$p=20$	$p=50$	$p=100$	$p=\infty$
f_1	60.64	60.15	59.84	58.71	59.25	58.43	57.78	56.80
f_2	76.77	76.23	75.91	74.27	73.68	72.99	72.55	71.90
f_3	115.49	114.54	113.95	111.84	113.01	111.40	110.10	108.17
f_4	154.07	152.72	151.89	149.23	151.69	149.33	147.34	144.32
f_5	170.55	169.33	168.58	164.94	164.10	162.46	161.35	159.75
f_6	215.38	213.69	212.64	208.45	209.49	206.83	204.78	201.74
f_7	244.57	242.48	241.19	236.82	239.98	236.44	233.50	229.08
f_8	283.57	281.19	279.72	274.59	277.93	273.90	270.59	265.61
f_9	289.98	287.60	286.13	280.78	283.54	279.59	276.40	271.62
f_{10}	302.10	299.50	297.89	292.63	296.72	292.31	288.62	282.97

ACCEPTED MANUSCRIPT

Table 4. The first ten frequencies for the functionally graded parabolic panel (C-F-F-F) as a function of the power-law exponent p, for $a=1, b=0.5, c=3$.

$FGM_{1\,(a=1/b=1/c=3/p)}$ power-law distribution								
Frequencies [Hz]	$p=0$	$p=0.6$	$p=1$	$p=5$	$p=20$	$p=50$	$p=100$	$p=\infty$
f_1	60.64	61.18	61.48	62.43	60.07	58.40	57.66	56.80
f_2	76.77	76.86	76.87	76.22	74.07	72.96	72.48	71.90
f_3	115.49	116.58	117.20	119.29	114.67	111.33	109.86	108.17
f_4	154.07	156.00	157.06	160.90	154.31	149.24	146.97	144.32
f_5	170.55	170.94	171.11	170.51	165.34	162.44	161.19	159.75
f_6	215.38	216.88	217.69	219.93	212.07	206.75	204.43	201.74
f_7	244.57	247.25	248.73	253.90	243.83	236.32	232.97	229.08
f_8	283.57	286.52	288.15	293.66	282.21	273.76	270.00	265.61
f_9	289.98	292.68	294.17	298.94	287.60	279.44	275.83	271.62
f_{10}	302.10	305.58	307.46	313.13	301.21	292.11	287.93	282.97
$FGM_{2\,(a=1/b=1/c=3/p)}$ power-law distribution								
Frequencies [Hz]	$p=0$	$p=0.6$	$p=1$	$p=5$	$p=20$	$p=50$	$p=100$	$p=\infty$
f_1	60.64	61.16	61.44	62.31	59.99	58.36	57.64	56.80
f_2	76.77	76.83	76.83	76.11	74.00	72.93	72.46	71.90
f_3	115.49	116.54	117.12	119.07	114.52	111.26	109.83	108.17
f_4	154.07	155.93	156.95	160.57	154.08	149.13	146.91	144.32
f_5	170.55	170.88	171.01	170.20	165.12	162.33	161.13	159.75
f_6	215.38	216.79	217.56	219.51	211.77	206.61	204.35	201.74
f_7	244.57	247.14	248.56	253.39	243.47	236.14	232.88	229.08
f_8	283.57	286.40	287.96	293.09	281.81	273.56	269.89	265.61
f_9	289.98	292.57	293.98	298.38	287.21	279.25	275.72	271.62
f_{10}	302.10	305.45	307.26	312.59	300.82	291.92	287.83	282.97

ACCEPTED MANUSCRIPT

Table 5. The first ten frequencies for the functionally graded parabolic toroid (F-C) as a function of the power-law exponent p, for $a = 0, b = -0.5, c = 2$.

$FGM_{1\,(a=0/b=-0.5/c=2/p)}$ power-law distribution								
Frequencies [Hz]	$p = 0$	$p = 0.6$	$p = 1$	$p = 5$	$p = 20$	$p = 50$	$p = 100$	$p = \infty$
f_1	52.59	52.37	52.24	51.47	51.16	50.99	50.77	49.26
f_2	52.59	52.37	52.24	51.47	51.16	50.99	50.77	49.26
f_3	59.27	58.97	58.79	57.79	57.75	57.75	57.56	55.52
f_4	59.27	58.97	58.79	57.79	57.75	57.75	57.56	55.52
f_5	59.69	59.46	59.32	58.47	58.08	57.85	57.58	55.91
f_6	59.69	59.46	59.32	58.47	58.08	57.85	57.58	55.91
f_7	74.38	74.04	73.83	72.53	72.61	72.53	72.24	69.66
f_8	74.76	74.29	73.99	72.53	73.01	73.36	73.21	70.03
f_9	74.77	74.29	74.00	72.68	73.01	73.36	73.22	70.03
f_{10}	96.51	95.78	95.33	93.20	94.42	95.26	95.17	90.39
$FGM_{2\,(a=0/b=-0.5/c=2/p)}$ power-law distribution								
Frequencies [Hz]	$p = 0$	$p = 0.6$	$p = 1$	$p = 5$	$p = 20$	$p = 50$	$p = 100$	$p = \infty$
f_1	52.59	52.28	52.09	51.05	50.70	50.61	50.47	49.26
f_2	52.59	52.28	52.09	51.05	50.70	50.61	50.47	49.26
f_3	59.27	58.86	58.62	57.34	57.24	57.34	57.20	55.52
f_4	59.27	58.86	58.62	57.34	57.24	57.34	57.20	55.52
f_5	59.69	59.34	59.12	57.94	57.50	57.37	57.24	55.91
f_6	59.69	59.34	59.12	57.94	57.50	57.37	57.24	55.91
f_7	74.38	73.84	73.52	71.83	71.65	71.74	71.61	69.67
f_8	74.76	74.15	73.78	71.95	72.38	72.85	72.80	70.03
f_9	74.77	74.15	73.78	71.95	72.38	72.85	72.81	70.04
f_{10}	96.51	95.60	95.06	92.47	93.62	94.60	94.65	90.40

ACCEPTED MANUSCRIPT

Table 6. The first ten frequencies for the functionally graded parabolic dome (C-F) as a function of the power-law exponent p, for $a = 0.8, b = 0.2, c = 3$.

$FGM_{1\,(a=0.8/b=0.2/c=3/p)}$ power-law distribution								
Frequencies [Hz]	$p=0$	$p=0.6$	$p=1$	$p=5$	$p=20$	$p=50$	$p=100$	$p=\infty$
f_1	125.16	124.31	123.78	122.15	120.81	119.14	118.29	117.23
f_2	125.16	124.31	123.78	122.15	120.81	119.14	118.29	117.23
f_3	171.58	170.40	169.66	165.63	162.83	161.72	161.25	160.72
f_4	171.58	170.40	169.66	165.63	162.83	161.72	161.25	160.72
f_5	179.28	178.06	177.29	175.08	173.28	170.80	169.52	167.93
f_6	179.28	178.06	177.29	175.08	173.28	170.80	169.52	167.93
f_7	207.82	206.41	205.53	201.30	198.19	196.43	195.62	194.66
f_8	220.98	219.46	218.50	216.48	214.70	211.17	209.32	206.99
f_9	220.99	219.47	218.51	216.49	214.71	211.18	209.33	206.99
f_{10}	225.61	224.07	223.10	219.28	216.40	213.97	212.77	211.32
$FGM_{2\,(a=0.8/b=0.2/c=3/p)}$ power-law distribution								
Frequencies [Hz]	$p=0$	$p=0.6$	$p=1$	$p=5$	$p=20$	$p=50$	$p=100$	$p=\infty$
f_1	125.16	123.96	123.25	121.17	120.34	118.93	118.18	117.23
f_2	125.16	123.96	123.25	121.17	120.34	118.93	118.18	117.23
f_3	171.58	170.07	169.16	164.75	162.41	161.52	161.15	160.72
f_4	171.58	170.07	169.16	164.75	162.41	161.52	161.15	160.72
f_5	179.28	177.58	176.55	173.72	172.62	170.49	169.36	167.93
f_6	179.28	177.58	176.55	173.72	172.62	170.49	169.36	167.93
f_7	207.82	205.92	204.79	199.93	197.53	196.13	195.46	194.66
f_8	220.98	218.86	217.58	214.77	213.86	210.79	209.12	206.99
f_9	220.99	218.87	217.59	214.78	213.87	210.80	209.13	206.99
f_{10}	225.61	223.52	222.27	217.74	215.66	213.63	212.60	211.32

Table 7. The first ten frequencies for the functionally graded toro-parabolic panel (C-F-C-F) for an increasing the number of grid points $N = M$ of the Chebyshev-Gauss-Lobatto distribution.

$FGM_{1\,(a=1/b=0/c=0/p=5)}$ power-law distribution							
Frequencies [Hz]	$N=M=11$	$N=M=15$	$N=M=17$	$N=M=21$	$N=M=25$	$N=M=29$	$N=M=31$
f_1	98.12	99.18	99.17	99.14	99.13	99.12	99.12
f_2	101.71	102.70	102.71	102.71	102.71	102.72	102.72
f_3	109.11	110.16	110.18	110.20	110.20	110.20	110.20
f_4	129.04	128.96	128.92	128.87	128.84	128.83	128.83
f_5	154.10	155.43	155.50	155.55	155.56	155.56	155.56
f_6	181.86	181.65	181.60	181.53	181.50	181.49	181.49
f_7	188.10	189.01	189.05	189.07	189.07	189.07	189.07
f_8	191.16	189.96	189.92	189.88	189.86	189.85	189.85
f_9	198.51	199.81	199.85	199.86	199.86	199.86	199.86
f_{10}	203.82	204.87	204.91	204.91	204.92	204.92	204.92

ACCEPTED MANUSCRIPT